J. Fluid Mech. (1970), *vol.* 40, *part* 3, *pp.* 603–640
Printed in Great Britain

Inertial oscillations in a rotating fluid cylinder

By A. D. McEWAN

C.S.I.R.O. Division of Meteorological Physics,
Aspendale, Victoria 3195, Australia

(Received 11 March 1969)

A study is described of the forced inertial oscillations appearing in an axially rotating completely filled circular cylinder with plane ends. Excitation is provided by causing the top end to rotate about an axis inclined slightly to the rotation axis. Experiments demonstrate the presence of numerous low mode resonances in a densely spaced range of ratios of net cylinder height to radius in close conformance with linear inviscid theory. Where geometry permits simple corner reflexion, characteristic surfaces are revealed which confirm in part the theoretical predictions concerning their scale and form.

Detailed measurements are given of the amplitude at one point within the cylinder for the condition in which the disturbance frequency equals the rotation frequency. Amplitude column height spectra are compared with theoretical estimates, and the evolution of amplitude for the simplest mode of resonant oscillation is studied. A non-linear theory based on the integral energy of large amplitude oscillation is derived whose broad features are in fair quantitative and qualitative agreement with these observations.

Some investigation is made of the phenomenon of *resonant collapse*, in which larger amplitude resonant oscillations, after persisting in an apparently laminar form, degenerate abruptly into a state of agitation and disorder from which they do not recover. It is found that the time for emergence of this collapse after the introduction of the forcing disturbance has a close correspondence with the theoretical period of one 'evolutionary' cycle of momentum exchange between the main motion and the secondary oscillation.

1. Introduction

It is well known that inertial oscillations with a frequency less than twice the basic rotation Ω can exist within a fluid in uniform rotation. When the fluid is confined within cylindrical boundaries resonant amplification of axially periodic disturbances of a frequency related to discrete values of the ratio of column length l to radius a, is predicted in the inviscid limit. These oscillations were anticipated first by Kelvin (1880) and were re-examined by Bjerknes, Bjerknes, Solberg & Bergeron (1933).

One of the more familiar manifestations of inertial resonance is the instability of liquid filled gyroscopes or spinning projectiles (Stewartson 1959), for which the greatest rate of growth in nutation amplitude is experienced when the nutational frequency is the same as that of the simplest free inertial mode (e.g. Karpov 1965).

More direct studies have been made of the oscillations themselves. Fultz (1959) confirmed the presence of several of the simpler modes by observing the dispersion of dye in a rotating cylinder excited by an axially oscillating plane disk. Johnson (1967) calculated the first-order viscous correction to resonant column geometry and observed primary resonance in a precessing liquid-filled cylinder.

Recently attention has been directed to the case of spherical boundaries for which excitation is derived from periodic entrainment in the boundary layers. Experiments by Aldridge & Toomre (1969) on a rotating liquid filled sphere subjected to periodic angular perturbation nicely confirmed calculations based on Greenspan's (1964) expansions for motion in a viscous rotating fluid. Malkus reported observations in a precessing spheroid, noting the presence of a steady westwards circulation (see Bretherton, Carrier & Longuet-Higgins 1966, p. 407); these were accounted for by Busse (1968) as a second-order effect of boundary-layer oscillation.

The equations for inviscid perturbed fluids in rotation are hyperbolic in the range of frequency σ giving rise to the oscillations implying that disturbances originating at boundary discontinuities will be transmitted without attenuation through the bulk of the fluid along conical characteristic surfaces inclined at $\arcsin(\sigma/2\Omega)$ to the rotation axis. Physically these discontinuities are recognized as resulting from the coincident flow contributions, of an infinite sum of forced inertial modes decreasing in scale, but of equal frequency. Wood (1965) estimated the magnitude of the individual modes, establishing that the characteristics from the corners of a cylinder precessing at a small angle to the rotation axis, provided they ultimately re-reflected upon themselves, were realized as discontinuities in velocity or in velocity gradient, depending upon the geometry of the reflexion. Baines (1966) repeated Wood's calculations for a cylinder in axial rotation whose top is deformed in a periodic fashion to retain a fixed form relative to a stationary observer, thereby introducing a disturbance with harmonic frequencies of the basic rotation. Oser (1958) has made experimental confirmation of the presence of characteristic surfaces in a rotating suspension of aluminium powder, perturbed by an axially oscillating visible disk. Conical surfaces from the intense edge disturbance were seen to be at the theoretical angle to the rotation axis, but no boundary reflexions were detected.

Notwithstanding these observations there arise from the linearized inviscid solutions for cylindrically *bounded* motions features of questionable physical validity. The disturbance pressure emerges as an infinite sum of axi-symmetric modes as described by equation (1.2). Resonance occurs for any integral value of $\lambda_s l\sigma/\pi(4\Omega^2-\sigma^2)^{\frac{1}{2}}a$, the roots λ_s being related such that resonant ratios of column length l to radius a are densely spaced; thus the solution changes discontinuously with this ratio. In the absence of resonance an infinitesimal change in column length may change the distribution of characteristic surfaces within the container from one in which the surfaces reflect upon themselves $(l\sigma/4\Omega^2-\sigma^2)^{\frac{1}{2}}a =$ (a rational fraction) to one for which an infinite number of reflexions occur and the characteristics are never retraced.

In relation to real fluids these difficulties might be regarded as artificial in that

viscosity would be expected to act to attenuate the modes of finer scale to moderate discontinuous changes with boundary conditions. Greenspan (1968) regards the presence of imaginary contributions to λ of order R^{-1} (R being the Reynolds number defined as $\Omega a^2/\nu$) as capable of invalidating the inviscid solution for the modes of higher wave-number than $O(R^{\frac{1}{2}})$. However, Wood (1966) established for his original configuration that, for large R, the inviscid solution is indeed a true approximation to the real fluid motion but that internal shear discontinuities are realized in strength $O(R^{\frac{1}{6}})$ over layers $O(R^{-\frac{1}{3}})$ in thickness. According to Wood, for small departures from rational values of $l\sigma/\Omega(4\Omega^2-\sigma^2)^{\frac{1}{2}}a$ there is little diminution in the strength of reflected layers parallel to the 'original' unless $R^{\frac{1}{6}} \gg \ln R$, provided $R^{-1}T^3$ is small where T is an integer related to the number of reflexions occurring on the top and bottom surfaces (see §1.2), a condition which cannot be met on an experimental scale. Baines (1967) has noted for an impulsively started axial oscillation of a right cylindrical container that the emergence of characteristic discontinuities is contingent on the viscous decay of initial modes, and inferred from this that the inviscid form of the 'steady' forced motion should only be approached in a *viscous* medium.

These last two observations are curious in the sense that the greatest departure from 'steady' inviscid conditions is expected at the highest Reynolds number (a situation finding many parallels) and places in question the relevance of a 'steady' or final state description, quite apart from possible effects of finite amplitude of secondary motion, boundary-layer advection shear layer stability and the like.

Some experimental evidence already exists to suggest that steady motion is not in fact sustained *near resonance*. Johnson identified the simplest mode resonance by the emergence of a 'turbulent looking' pattern; of Malkus' work the feature regarded as *most significant* was that, above a critical Reynolds number, the zonal circulation became unstable and could degenerate to violent disorder beyond a certain precession frequency. Malkus suggested that if the same kind of behaviour were to occur in the Earth's magma, the precessional torques acting in the presence of the disorder might be of a magnitude sufficient to sustain terrestrial magnetism. Even in the study of the dynamics of liquid gyroscopes there is some evidence of transition to disorder when critical conditions are exceeded; in the evolution of nutational instability Karpov noted that after an initial exponential growth according well with linear theory, there was an abrupt drop and subsequent unsteadiness in the rate of increase of amplitude at resonance.

The present experiments were undertaken to define the character of forced disturbances in a real rotating system with a view to establishing the validity of small amplitude inviscid descriptions, to verify estimates of the influence of viscosity in modifying these descriptions and to find the part played by nonlinear effects arising from the finite amplitude of the secondary motion when resonance is encountered. It was revealed that the processes of evolution of oscillation of large amplitude at resonance were subject to effects making inadequate use of the linear theory, and which are apparently not amenable to rigorous analysis, but the experiments also suggested the physical processes

by which the motion is sustained. An equation representing the gross features of these processes in the form of an energy balance was posed and its solution showed a moderate consistency with observations of both resonant growth and collapse. One of the implications is that if constraints to the oscillation imposed by viscosity are exceeded, a truly 'steady state' of oscillation may be physically unattainable.

1.1. *Features of the inviscid analysis*

Reference is made to figure 1. A right circular cylinder of radius a and height l contains liquid in uniform axial rotation $\Omega\mathbf{z}$. The liquid is enclosed by a plane top which rotates at a rate Ω about an axis inclined at a slight angle α to $\mathbf{z}$, which intersects $\mathbf{z}$ in the plane of the top. This axis may precess at a rate Ω_1, relative to a fixed frame. Secondary motion is imposed upon the primary rotation of the liquid by the relative precession of the top. The net volume of the container remains constant.

In a cylindrical co-ordinate system rotating at Ω_1 the linearized equations for secondary motion $\mathbf{q}(r, \phi, z, n)$ are

$$\left.\begin{aligned} \frac{\partial \mathbf{q}}{\partial n} + \frac{\partial \mathbf{q}}{\partial \phi} + 2\omega\hat{\mathbf{z}} \times \mathbf{q} &= -\nabla P, \\ \operatorname{div} \mathbf{q} &= 0, \end{aligned}\right\} \tag{1.1}$$

where $n = \sigma\tau$, dimensionless time, and P is the reduced hydrostatic pressure, $(P/\rho - \frac{1}{2}\Omega^2 r^2)(\Omega - \Omega_1)$. The frequency of the disturbance is $\sigma = (\Omega - \Omega_1)$ and $\omega = \Omega/\sigma$. The boundary conditions for motion (u, v, w) resolved in the r, ϕ, z directions are

$$\left.\begin{aligned} u &= 0 \quad \text{at} \quad r = a, \\ w &= 0 \quad \text{at} \quad z = 0, \\ w &= \alpha\sigma r \cos\phi \quad \text{at} \quad z = l. \end{aligned}\right\} \tag{1.1a}$$

The equations are solved by methods similar to those outlined elsewhere (Wood 1965; Baines 1967); solutions pertinent to the present study are as follows:

(i) For forced motion steady relative to the disturbance

$$P_s = -2\alpha\sigma(4\omega^2 - 1)^{\frac{1}{2}}(2\omega + 1)a^2 \sum_{s=1}^{\infty} \frac{J_1(\lambda_s r/a)\cos(\lambda_s z/(4\omega^2 - 1)^{\frac{1}{2}}a)\sin\phi}{\lambda_s(\lambda_s^2 + 4\omega^2 - 1)J_1(\lambda_s)\sin(\lambda_s l/(4\omega^2 - 1)^{\frac{1}{2}}a)}, \tag{1.2}$$

where λ_s is the sth positive root of

$$\lambda J_0(\lambda) + (2\omega - 1)J_1(\lambda) = 0. \tag{1.2a}$$

In this case the disturbance motion

$$\mathbf{q} = U\mathbf{r}\cos\phi + V\boldsymbol{\phi}\sin\phi + W\mathbf{z}\cos\phi$$

is given by

$$\left.\begin{aligned} U &= -(\partial P_s/\partial r + 2\omega P_s/r)/(4\omega^2 - 1), \\ V &= -(2\omega\,\partial P_s/\partial r + P_s/r)/(4\omega^2 - 1), \\ W &= \partial P_s/\partial z. \end{aligned}\right\} \tag{1.3}$$

The intensity of the motion becomes indeterminate and the contribution of each

mode s changes in phase by π as the cylinder height l attains successive resonant values,

$$l = \pi(4\omega^2 - 1)^{\frac{1}{2}} am/\lambda_s, \tag{1.4}$$

where m is an integer. Each resonant mode is identified by the root λ_s and m the number of axial repetitions (for instance $\lambda_2 m_3$). Boundary discontinuities produce along characteristic surfaces disturbances whose nature is identified by

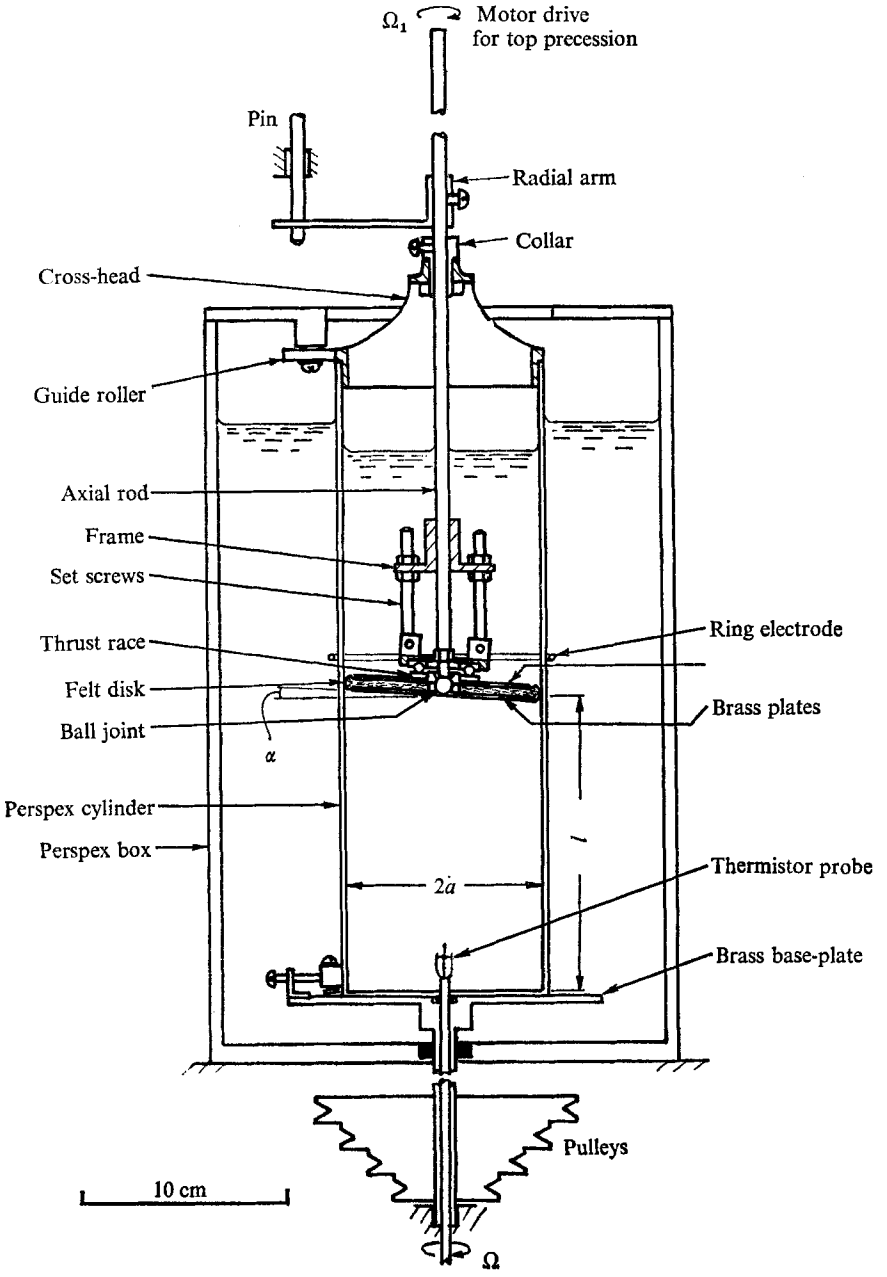

FIGURE 1. Cylinder arrangement, viewed in section $\phi = \frac{1}{2}\pi$.

considering the summation of (1.2) as $s \to \infty$. These disturbances must retrace themselves after finite reflexions if

$$l/a(4\omega^2 - 1)^{\frac{1}{2}} = B/T, \tag{1.5}$$

where B and T are coprime integers.

Estimation of the magnitude of the summation of the higher (large s) modes enables the strength of the characteristic discontinuities to be calculated.

The discontinuity is in velocity gradient ($O(s^{-3})$ in P), except when

$$B/T = 4\zeta/(1+2\xi), \tag{1.6}$$

where ζ and ξ are integral, for which case the discontinuity ($O(s^{-2})$ in P) is in velocity. The discontinuities occur across surfaces $\beta\pm$ = constant where

$$\beta\pm = (r/a \pm B/T\, z/l) \tag{1.7}$$

and substitution in the motion equations establishes that the component or the gradients of the component of velocity normal to these surfaces are continuous but that the discontinuity exists either in the component of velocity or of normal gradient of velocity tangential with β surfaces and inclined to the constant ϕ lines on these surfaces at an angle $(\frac{1}{2}\pi + \phi)$.

(ii) For free and forced oscillation after a sudden change, at $n = 0$, of the top plane from an attitude $z = l + r\sin\phi$ fixed relative to a frame rotating at $\boldsymbol{\Omega}$, to an attitude fixed in space. For $n = 0+$, $\omega = 1$ and if the cylinder height l is such that one of the steady modes defined by (1.2a) and 1.4 is resonant, then relative to a spatially fixed frame

$$\begin{aligned} P = P_s(\underset{(\mathrm{I})}{\text{non resonant}}) - 6\sqrt{3}\,\alpha\Omega a^2 \sum_{s=1}^{\infty} \frac{J_1(\lambda_s r/a)}{\lambda_s(\lambda_s^2+3)\,J_1(\lambda)} \Big\{ \frac{3(-1)^M}{4\pi M} \Big[n\cos\phi \underset{(\mathrm{II})}{\cos}\left(\frac{M\pi z}{l}\right) \\ - 4M\pi z \underset{(\mathrm{III})}{\sin\phi}\sin(M\pi z/l)/3\sqrt{3}l - \underset{(\mathrm{IV})}{\sin\phi}\cos(M\pi z/l)/3 \\ + \tfrac{1}{2}\underset{(\mathrm{V})}{\sin}(2n-\phi)\cos(M\pi z/l)\Big] + \sum_{m\neq M} \frac{(-1)^{m+1}(4-\gamma_M^2)^2}{2(\lambda_s l/a)\,(1-\gamma_m^2)} \\ \times \frac{\cos(\lambda_s z/\sqrt{3}a)}{\sin(\lambda_s l/\sqrt{3}a)} \underset{(\mathrm{VI})}{[\gamma_m \sin(\gamma_m n)}\underset{(\mathrm{VII})}{\cos(\phi - n) + \cos(\gamma_m n)\sin(\phi - n)}] \Big\}, \end{aligned} \tag{1.8}$$

where

$$\gamma_m(s) = 2m\pi/((\lambda_s l/a)^2 + m^2\pi^2)^{\frac{1}{2}} \tag{1.9}$$

and

$$M = \lambda_s l/\pi\sqrt{3}a$$

is integral.

The velocity field is defined by

$$\left.\begin{aligned} \left(\left(\frac{\partial}{\partial n} + \frac{\partial}{\partial\phi}\right)^2 + 4\right) u &= \begin{vmatrix} -\dfrac{\partial p}{\partial r} & -2 \\ -\dfrac{\partial p}{r\,\partial\theta} & \left(\dfrac{\partial}{\partial n} + \dfrac{\partial}{\partial\phi}\right) \end{vmatrix}, \\ \left(\left(\frac{\partial}{\partial n} + \frac{\partial}{\partial\phi}\right)^2 + 4\right) v &= \begin{vmatrix} \left(\dfrac{\partial}{\partial n} + \dfrac{\partial}{\partial\phi}\right) & -\dfrac{\partial p}{\partial r} \\ 2 & -\dfrac{\partial p}{r\,\partial\phi} \end{vmatrix}, \\ \left(\frac{\partial}{\partial n} + \frac{\partial}{\partial\phi}\right) w &= -\frac{\partial p}{\partial z}. \end{aligned}\right\} \tag{1.10}$$

The terms in (1.8) are, respectively, steady forced modes, growing and steady free resonant modes, initial resonant and non-resonant free modes.

Substitution of (1.8) into the first of the equations establishes that the radial component of velocity on the axis, arising from the *resonant mode alone* is

$$u(0,\phi,z,n) = -\frac{3\sqrt{3}\,(-1)^M \alpha\Omega a}{4\pi M(\lambda^2+3)J_1(\lambda)}\left[[3n\sin\phi - 2\cos\phi + \cos(2n-p)]\cos\left(\frac{m\pi z}{l}\right) + \frac{4m\pi z}{\sqrt{3}\,l}\cos\phi\sin\frac{m\pi z}{l}\right]. \quad (1.11)$$

2. Experiments

2.1. *The cylinder*

The experiments were performed on a vertically mounted Perspex cylinder machined within $\pm 0{\cdot}1\,\%$ to 4·73 cm internal radius, and having a height of about 30 cm. This was mounted in a rectangular Perspex box and both vessels were filled with mineral turpentine, chosen for its low viscosity (1·064CS at 20 °C) and a refractive index close to that of Perspex. The cylinder was rotated about its axis on a shaft driven through interchangeable pulleys by a compound motor on a stabilized a.c. supply or by a three-phase induction motor.

To simulate as closely as possible the theoretical conditions for the forcing disturbance, the top of the cylinder enclosing the liquid column was arranged in the following way. Reference is made to figure 1. The top was formed from a close fitting felt disk sandwiched between two brass plates of slightly smaller size. A ball joint at the axis of the plates and enclosed between them connected to an axial rod which bore a collar and a radial arm. The collar turned freely in a cross-head mounted on the top of the cylinder. This cross-head through the collar took the weight of the rod and the top and served to minimize the relative axial motion of the axis of the top and the cylinder.

On the upper plate of the top was fitted a thrust race bearing against a frame also mounted on the axial rod. Set screws on this frame enable the upper part of the race to be tilted relative to the rod axis, constraining the top to a rational freedom about an axis inclined to the rod axis, these axes intersecting in the plane of the top.

Friction between the felt disk and the cylinder wall caused the top to rotate at a rate indistinguishable from that of the cylinder. The axial rod could be arrested by engaging the radial arm with a pin on the frame of the apparatus, or it could be rotated relative to the frame through a separate motor drive. Thus, while the boundaries confining a cylindrical liquid column of constant volume all revolved at a sensibly constant rate, the axis of the top could be made to precess at a different rate.

The pin engaging the radial arm could be withdrawn, permitting the whole assembly to rotate freely with the cylinder. In this condition the top introduced no disturbance to the basic rotation of the fluid inside. By moving the rod on the cross-head collar the column height could be raised to 24 cm.

2.2. *Visualization of the secondary motion*

Forced secondary motions are predicted to be steady relative to a frame stationary relative to the top axis. For most of the experiments this frame was stationary in space. The fluid in the cylinder was illuminated in a vertical diametral band about 1·0 cm wide by light from a mercury vapour source. Photographs were taken by a camera located on a normal to the illuminated plane.

Particle paths of the primary solid body rotation intersected the light beam parallel with the camera axis, and so would appear as dots. The secondary motion conferred a motion in the beam plane but the illumination period was limited by the beam width. Therefore conventional time exposures of suspended particles could not reveal by particle paths secondary motion of magnitude small compared with the primary. Such exposures, using very weak suspensions of particles, were used only to compare experimental and theoretical patterns of the lowest secondary modes.

The main visualizations were made using a pearlescent suspension of *Merlin AC* particles. These are mica flakes 0·5 μm thick, 5–20 μm diameter, coated with titanium dioxide to raise their refractive index. The finest particles were separated by sedimentation and introduced to the cylinder to make a suspension appearing slightly cloudy in ordinary light ($\sim$ 10 mg/l).

Observed variations in the light reflected evidently resulted from the tendency of the particles to occupy preferred orientations relative to the viscous stress field (see e.g. Goldsmith & Mason 1962). The particles were individually too small to be identified, but *en masse* they revealed a constant visible pattern when caused by a stress field stationary to the observer, though the particles forming the pattern were in flux through the illuminated band. The alignment of the particles could be biased to a particular attitude by imposing a d.c. electric field of about 1 kV/cm. It was found that characteristic patterns were revealed most clearly by applying a vertical field between a ring electrode encompassing the cylinder in a plane a few centimetres above the top, and the metal base plate. Tests ensured that this field itself did not impose a forcing disturbance on the fluid.

Notwithstanding the care taken to ensure a constant rotation speed, and in the fitting and alignment of the apparatus, some irregularity (a vertical striation with a period of about Ω^{-1}) persisted in the pattern even without deliberate disturbance. Its appearance suggested a two-dimensional, cylindrical eddy of simple form moving very slowly relative to the solid rotation. The electric field made the striation less visible, but did not appear to suppress the motion causing it. With the introduction of a forcing disturbance this 'background' pattern appeared to be dominated if the amplitude of the secondary motion was sufficiently great. Only at non-resonant cylinder heights did it obscure the 'forced' pattern sought.

2.2.1. *Visual evidence of resonance for* $\sigma = \Omega$ ($\Omega_1 = 0$). An observation was made of the patterns appearing in the fluid for a closely spaced range of column heights between 2·1 cm and 24·6 cm. In each case the procedure was to permit the top assembly to turn freely with the cylinder till the solid rotation was established.

The pin was then dropped to engage the radial arm, thus stopping the top axis at a preselected phase position relative to the camera. The pattern was photographed after a suitable interval.

Figure 2 (*a*)–(*o*) (plates 1 and 2) is representative of those obtained before unsteadiness appeared in the pattern. The time elapsed after the introduction of the disturbance is indicated. These were obtained with a cylinder rotation $\Omega = 23{\cdot}3$ rad/sec anticlockwise viewed from above and a top slope $\alpha = 0{\cdot}0344$. Illumination for these and all subsequent figures was from the right, and the plane $\phi = 0$ was located in the left of the illuminated band. The geometrical conditions may be located within the inviscid resonance spectrum by reference to figure 12. A more complete presentation of patterns is given elsewhere (McEwan 1968).

At each height corresponding with a resonant mode of orders up to $\lambda_4 m_8$ and $\lambda_3 m_6$, a common feature of the observed pattern was a wavy axial core. The number of half waves in its length was found to equal the appropriate value of m, the only exceptions (e.g. figure 2 (*f*)) occurring when the wave pattern was modulated by a stronger adjacent mode.

The wavy core, while it persisted, was sensibly steady in position, though it grew, then appeared to wane, in amplitude. For some of the higher-order resonances, a pattern appeared not at the core but near the cylinder wall (figure 2 (*n*)).

The significance of the visible cores can be appreciated by considering the means by which they appear. As mentioned earlier, their appearance would imply a systematic viscous stress upon the fluid forming the core. A uniform horizontal motion $\mathbf{u}$ superimposed upon the vertical axial rotation Ω causes a displacement u/Ω of the centre of rotation in a direction $\boldsymbol{\Omega} \times \mathbf{u}$.

Only when the superimposed motion is uniform do the streamlines remain circular and coaxial, and in this circumstance no stress is experienced by the fluid. However, if the bounded perturbation motion of (1.2) is superimposed, a fluid particle has a non-circular orbit displaced from the axis, and it experiences a spacially fixed stress. Thus, existence of a non-uniform secondary motion is implied by the appearance of a visible core; its *magnitude* is indicated by the size of the waves in the core, if 'sectioned' appropriately by the light beam. Furthermore, if the secondary motion is composed of a number of uncoupled modes of different characteristic size, the mode appearing most clearly should be that associated with the greatest viscous stress. As will be seen in later sections, the fundamental modes dominate in amplitude those of higher order, even for resonances remote from the fundamental, yet it is noted here that the higher-order modes are revealed in the visualization, evidently because these cause the greater aligning stresses.

The patterns may therefore be reasonably interpreted as evidence of appropriate resonant modes. The discrete existence of a relatively large number of such modes, each possessing a cell height predicted accurately by inviscid theory, is striking indeed, particularly in view of the density of the spectrum and the low Reynolds number of the experiment. Consecutive cell heights differing by as little as 0·13 of cylinder radius revealed different modes. Perhaps more impressive in this respect was the *absence* of coherent core distortions for *non-resonant* heights (figure 2 (*h*), (*i*), (*m*)).

A weak suspension of aluminium particles was used to reveal particle paths. For the lowest mode ($\lambda_1 m_1$) resonance, the short visible paths, where they could be distinguished, were found to conform well to the streamline section of the inviscid solution, when viewed in a light beam sectioning the $\phi = -\frac{1}{6}\pi$, $+\frac{5}{6}\pi$ plane. Higher mode resonances and characteristic surfaces were almost unrecognizable by this means of visualization.

2.2.2. *Characteristic discontinuity patterns.* It will have been noticed in some of the figures 2 that diagonal bands of light and dark are seen to spring from the upper corners of the container. These appeared most clearly when the ratio of column length to radius was close to a low integral multiple or fraction of $\sqrt{3}$, which by (1.6) would correspond to the occurrence of corner characteristics reflected upon themselves. As precisely as could be measured, the bands were inclined at 30° to the rotation axis, and in some cases exhibited bottom and side

		Band appearance, left to right	
Rotation	ϕ	L.H. characteristic	R.H. characteristic
A.C.W.	0	Dark/light	Dark/light
from above	$-\frac{1}{2}\pi$	Not clearly visible	
	$-\pi$	Light/dark	Light/dark
	$-\frac{3}{2}\pi$	Not clearly visible	
C.W.	0	Dark/light†	Dark/light†
from above	$-\frac{1}{2}\pi$	Dark†	Dark/light†
	$-\pi$	†	Light/dark†

† Very indistinct.

TABLE 1

reflexion (e.g. figure 2(*c*), (*o*)). Secondary motion at resonant heights tended to obscure the bands, though it was found that a boundary disruption to this secondary motion, produced, e.g. by introducing a probe into the fluid through the axis at the bottom of the vessel (see figure 1), would radiate visible bands at the same angle. Lateral movement of the light beam confirmed that the bands delineated the diametral section of conical surfaces having reflecting properties different from the bulk of the fluid suspension; these surfaces were thus identified as characteristics.

In an attempt to identify the fluid strains causing the characteristics to be revealed in this manner, the phase of the top axis relative to the illuminated plane was varied through a full circle, with the experimental conditions as for figure 2(*k*) ($l/a = 2\sqrt{3}$). The observations were repeated for reversed rotation (clockwise viewed from above such that $\mathbf{L} \times \mathbf{z}$ was directed away from the camera, $\mathbf{L}$ being the light direction). In each case where they appeared, the top corner characteristics were adjacent bands of light and dark relative to the surrounding medium. A summary is given in table 1. It was noticed that the patterns were scarcely visible when the plane $\phi = \frac{1}{2}\pi, \frac{3}{2}\pi$ was illuminated, or when the rotation was *clockwise*.

From the observations a picture can be built up of the 'preferred' attitude of particles forming these adjacent bands, relative to a frame fixed with respect to

the direction of the discontinuity, as defined by the inviscid theory (final paragraph, § 1.2); letting x' and y' be tangent to the plane of the characteristic surface, parallel and normal to the discontinuity direction with z' having an r positive component, the particles seem to prefer altitudes in the planes,

$$x' - c|z'| - dy'\boldsymbol{\Omega}.\boldsymbol{\kappa}/\Omega = \text{const.}, \tag{2.1}$$

c and d are positive constants near unity. c is discontinuous through $z' = 0$. $\boldsymbol{\kappa}$ is the unit vector in the surface normal (z') direction.

If a fluid field has components of motion whose spatial gradients are continuous in all directions but one, then relative to the net motion on the discontinuity plane the stagnation streamlines on each side of the plane will meet at different angles to the plane. This is in accordance with the discrete change in c through $z' = 0$; it can be deduced that a plate-like particle in suspension traversing the vicinity of a free stagnation point experiences fluid strains tending to align a major axis with the departing stagnation streamline. Since the fluid field containing such a particle comprises this stagnation flow superimposed on a continuous flow, the experimental evidence of table 1 is taken to support to a *limited extent* predictions for the existence and direction of gradient discontinuities.

The observed dependence of preferred attitude upon $\boldsymbol{\Omega}$, which suggests a non-reversible contribution to the velocity field cannot, however, be explained on the above basis.†

For the configuration just discussed the velocity gradient discontinuities from the top corners are predicted to be finite. From patterns in figure 2(*c*) and (*o*) it is noted that when the discontinuity predicted is 'logarithmically infinite' the order of light and dark is 'mirrored' at the axis (so that on both sides the inside of the cone appears dark). One model for this observation can be found if it is taken that c in (2.1) changes discontinuously from a small to a large value through $z' = 0$. By the same arguments as above this accords with a change in velocity gradient *large* compared with the net motion. No attempt was made to view these latter patterns with varying ϕ, so the self-consistency of the model is untested.

The third type of discontinuity indicated in table 1 is in velocity, arising when $l/a = (4, 8 \text{ etc.})\sqrt{3}/(1, 3, 5 \text{ etc.})$. One of the simplest forms attainable with the present apparatus, $l/a = 8/\sqrt{3}$ was photographed and is compared with the theoretical array in figure 3 (plate 3). Mirroring at the axis is clearer than in the previously discussed cases, but other definite features are difficult to identify.

It should be remarked finally that an unsuccessful attempt was made to obtain directly a profile of velocity through characteristic surfaces within configurations of $l/a = 2\sqrt{3}$ and $8/\sqrt{3}$, using a thermistor probe (as described in § 3.1). No change in net amplitude of the oscillation could be associated definitely with the characteristics, and though the velocity spectrum showed some variation, the equipment was too unsophisticated to permit resolution.

2.2.2.1. *Reynolds number dependence.* A series of photographs of the patterns appearing in the configurations, $l/r = 2\sqrt{3}$, were taken at rotation rates which

† Shear stresses generated by weak azimuthal convection (q.v. § 3) might be responsible for the $\boldsymbol{\Omega}$ dependence.

varied between 4·2 and 37·8 rad/sec, other conditions being as in figure 2. The width of the characteristic bands was measured on the photographic negative using a micro-densitometer, representative bands being traversed laterally at several stations along their length. From the records, the width was measurable from the spacing between maxima or minima bounding the band region.

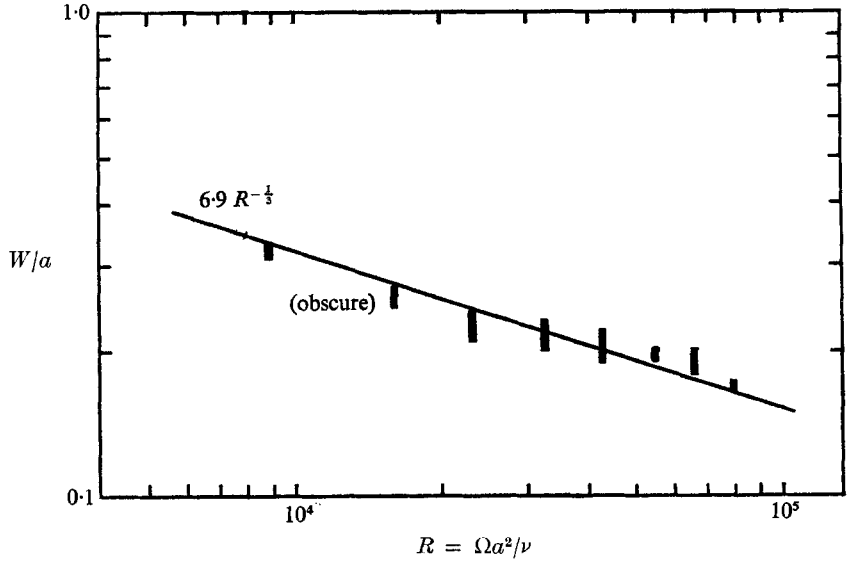

FIGURE 4. Width W of characteristic bands determined by microdensitometer traverses, as a function of Reynolds number.

In figure 4 the bars indicate the range of width measured over regions of the band. The results are seen to confirm roughly to a $-\frac{1}{3}$ power dependence upon Ω in support of Wood's predictions. It must be emphasized, however, that though the appearance of visible bands suggest localized strains in characteristic planes, a better understanding of how this comes about must precede definite quantitative conclusions concerning the actual width of the strained regions.

2.2.2.2. *Characteristics for variable* σ. To vary the frequency of the disturbance relative to the rotating frame the axial rod (figure 1) was rotated by a separate drive through a pulley and flexible coupling. Figure 5 is representative of the results. In each case a vertical electric field of about 1 kV/cm was applied, and the l/r ratio was adjusted wherever possible to avoid obscuration of the characteristic pattern by resonant motion. For these photographs the disturbance amplitude was 0·034, and the basic rotation was between 13 and 23 rad/sec, anticlockwise viewed from above.

In accord with the requirements for a hyperbolic solution to the motion equations, characteristic patterns only appear for $|\sigma/2\Omega| < 1$. Figure 5 (*a*) and (*i*) (plate 4) shows the appearance beyond this range. The disturbance motion could be observed by eye in these cases to diminish with distance from the top. In the conditions of figure 5 (*i*) oscillations immediately adjacent to the top could be seen to diffuse downwards. For $\sigma/2\Omega$ close to but less than unity (e.g.

figure 5(*b*)) it was found impossible to avoid an almost immediate growth and collapse of resonant oscillation, obscuring the characteristic pattern. The same thing did not occur with $\sigma/2\Omega$ close to -1 (the top precessing in the same direction as the base rotation) as in figure 5(*h*). A possible explanation is seen from (1.2), (1.2*a*) and (1.3): it is noted that the disturbance amplitude is much larger for positive than for negative values of this ratio, owing to the appearance of factors $(2\omega+1)$, and because, for negative $\omega \to -\frac{1}{2}$, the lowest eigenvalue λ_1 is approximately 5·135, compared with 2·405 for $\omega \to +\frac{1}{2}$.

As σ is reduced in magnitude the characteristic angle to the axis diminishes, and the bands become less distinct; for $|\sigma/2\omega| < 0{\cdot}2$ they cannot be identified accurately (figure 5(*e*)). Furthermore, the top corner characteristics tended to follow the top in its precession, and so appeared slightly unsteady to a fixed observer; thus the angular measurement could be considered accurate only to within the magnitude of the disturbance amplitude, $\pm 2°$.

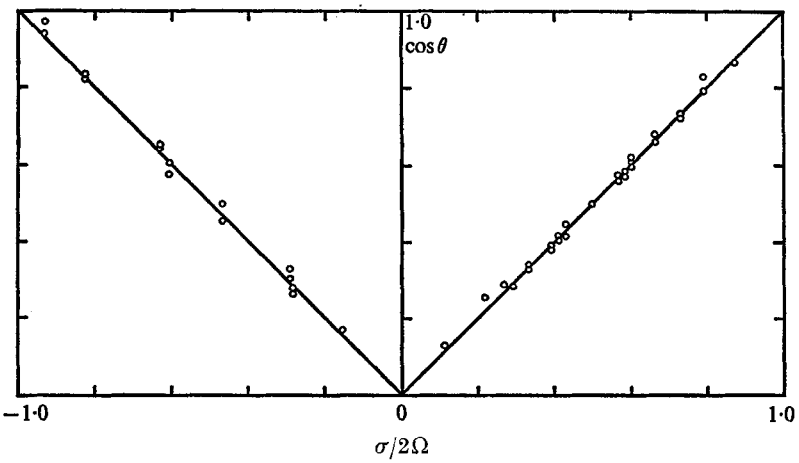

FIGURE 6. Characteristic surface angle θ to top surface. Dependence upon disturbance frequency σ.

Figure 6 shows the cosine of the characteristic angle measured relative to the top surface, as a function of disturbance frequency. Positive values of $\sigma/2\Omega$ correspond with top precessions that are less in sense than the basic rotation. It is seen that the theoretical angles are well confirmed.

2.2.2.3. *Multiple re-reflexion of characteristics.* Although quite complicated arrays of reflexion were at least partly visible for low rational values of $l/\sqrt{(3a)}$ as exemplified by figure 3, multiple reflexions for small departures from these values appeared very seldom, and only the main characteristics would be revealed. Noting from figure 4 that the 'thickness' of the discontinuity seemed to be about 0·2 in these figures, the change in l/a necessary to 'separate' the characteristics is 0·4, which is generally greater than the spacing between visible resonant modes. On the supposition that the clarity of the visible bands was an indication of the strength of the discontinuity, there was no evidence in support of Wood's prediction that for the present situation, in which $\ln R$ and $R^{\frac{1}{3}}$ are of the same order, the strength of reflected parallel layers should remain unchanged.

It is noted from the photographs, however, that individual characteristics *do* remain constant in strength along their length until they experience reflexion at the container surface or with other strong characteristics and this suggests that the attenuation may be due to local dissipation or distortion near the reflexion line. Such local effects are not accounted for in Wood's calculations based as they were on internal linear attenuation of individual modes through the whole fluid bulk.

2.2.3. *Visible evidence of resonant collapse,* $\sigma = \Omega$. On the introduction of the forcing disturbance in all configurations, the patterns as shown in figure 2 became visible and remained steady *in form* after the container had described a few revolutions. With resonant column lengths there would be some variation in the amplitude of waves in the core, but apart from an apparently uniform slow westwards convection (q.v. §3), very little evidence of secondary motion non-stationary with respect to an external observer. All of the photographs in figure 2 were taken during this 'steady' period at the times indicated. In the case of λ_1, λ_2 and λ_3 resonances however, and other isolated cases of higher λ, non-stationary and evidently periodic disturbances became apparent after some time, and grew rapidly to replace the previously steady pattern with one of disordered agitation. The abruptness with which the collapse to disorder took place, and the degree of subsequent agitation depended directly on the intensity of steady oscillation; after collapse a steady pattern was never fully regained, although the agitation waxed and waned.

The sequence of photographs in figure 7 (plate 5) and figure 8 (plate 6) show steady resonant growth and collapse of the $\lambda_1 m_2$ mode at high ($4{\cdot}8 \times 10^4$) and low ($7{\cdot}7 \times 10^3$) Reynolds number. The excitation amplitude α was 0·063. Unsteadiness could first be perceived by eye before figures 7(*e*) and 8(*f*) were taken. The kink in the visible core in figure 7(*e*) seemed to be associated with the intersection of the corner characteristic which can just be discerned. At the higher rotation speeds events in the collapse process occurred too rapidly to be discriminated by eye. At the lowest speeds, the collapse was protracted over several revolutions of the cylinder, and up to about 1·5 revolutions per second ($R = 1{\cdot}9 \times 10^4$) for conditions near resonance, there seemed to be three phases in the collapse:

(I) Unsteadiness was detected first in the upper and lower corners, appearing as a local fluctuation in brightness of the suspended particles whose period did not seem to be directly connected with the basic rotation. This grew rapidly in degree and extended through the whole cylinder (figure 8(*f*), (*g*), (*h*)); the visible core became distorted and sometimes axially striated before

(II) the pattern became completely disordered (figure 8(*i*)) the bands of fluctuating brightness becoming more extended axially. The core pattern would re-emerge vaguely but without complete suppression of the disorder.

(III) At higher rotation speeds the disorder appeared to degenerate to a finer scale, fully 'turbulent' in appearance, at the higher speeds this being almost concurrent with phase (II) (figure 7(*e*), (*f*), (*g*), (*h*)) the core pattern re-emerging periodically (figure 7(*i*)).

Weaker excitation protracted the steady oscillation period and made the collapse less dramatic. Collapse would also be avoided in all other configurations for sufficiently weak excitation or low rotation rate, depending upon the amplitude of the steady secondary oscillation of each particular mode.

So definite and reproducible was the emergence of the unsteady oscillation that the time to its appearance after the commencement of forcing could be measured or predicted quite accurately. Figure 9 shows the revolutions (i.e. $\Omega\tau/2\pi$) plotted against Ω for the $\lambda_1 m_2$ mode for four values of forcing amplitude α. In each case the leftmost point indicates the lowest value of Ω for which collapse could be identified with certainty.

Further discussion of the process of resonant collapse is reserved till §3.

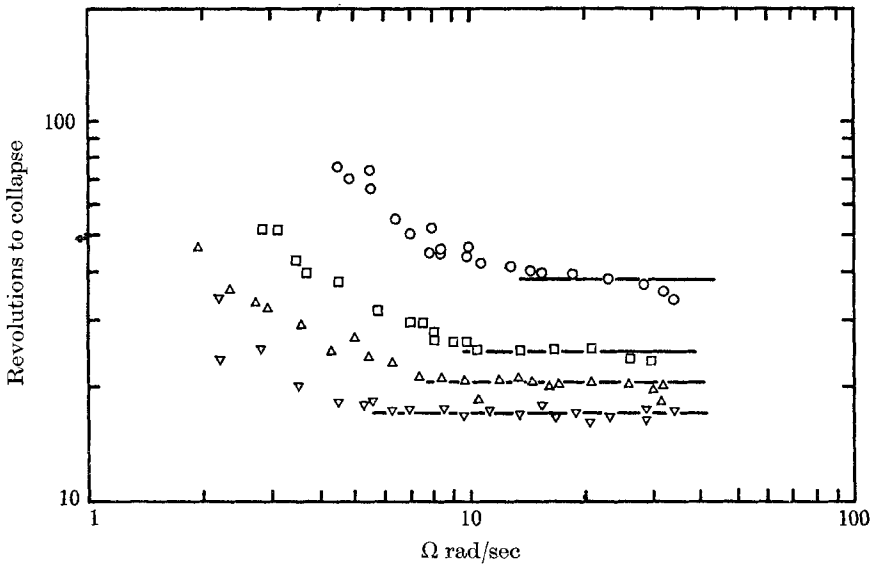

FIGURE 9. Revolutions of container till first appearance of unsteadiness preceding resonant collapse, $\lambda_1 m_2$ mode. ○, α = 0·0180; □, 0·0342; △, 0·0483; ▽, 0·0608.

2.3. *Measurement of the amplitude of the secondary motion*

The net amplitude of the secondary oscillation was measured using miniature thermistors (S.T.C. Type U 23) mounted on a fine wire fork on a probe feeding axially through a seal from the lower driving shaft (see figure 1). The thermistor leads connected through sliprings to a d.c. bridge whose output was monitored on a pen recorder. The bridge was without compensation, and it was considered necessary therefore to simulate closely in their calibration the conditions the thermistors would experience in the cylinder, namely a flow, which changed comparatively slowly in *magnitude*, but which *revolved* in direction about the thermistor at the rate of rotation of the container. This was achieved by calibrating the peak output from the bridge when the thermistors were made to describe circular *irrotational* motions of various angular velocities and radii in a tank of turpentine. Details of the method are given by McEwan (1968).

For most measurements described in the following pages a single thermistor mounted horizontally about 1·3 cm above the bottom and near the axis of rotation was used. To minimize interference only the support wires intruded into the cylinder. Vessel temperatures were carefully stabilized. Without forced motion the junction temperature within the thermistor was about 15 °C above the surroundings. In this position, the thermistor was most sensitive to velocities in the r–z plane and the calibration method avoided the necessity of determining separately their sensitivity to tangential motion, being based on the peak flow velocity normal to the thermistor axis relative to the *rotating* frame. In the locality of the thermistor when mounted in the cylinder the z component of velocity was always small so the measured quantity was effectively $U/\Omega a$.

2.3.1. *The evolution of oscillation amplitude.* The oscillation amplitude was plotted for a range of column configurations as a function of time after the introduction of a forcing disturbance stationary relative to a fixed observer ($\sigma = \Omega$). Figure 10 presents representative traces. For this figure the disturbance amplitude α was 0·0342 and $\Omega = 16{\cdot}9$ rad/sec, $R = 3{\cdot}48 \times 10^4$; each successive trace is separated on the ordinate by two decades in $U/\Omega a$. Tabulated below is the configuration to which each trace corresponds, numbered from the lowest trace.

Trace	l/a	Resonance, or rational char. reflexion
1	1·73	$B/T = 1$
2	1·99	$\lambda_1 m_1$
3	2·48	$\lambda_3 m_4$
4	2·95	—
5	3·98	$\lambda_1 m_2$
6	4·80	$\lambda_2 m_5$

TABLE 2

In traces 1, 3, 4 and 6 only a faired curve of the peak amplitude in each cycle as a function of time has been drawn for the sake of clarity. In traces 2 and 5 the full recorded trace has been reproduced in order to show how the resonant collapse is revealed in the record. The arrows indicate the time at which the spacial unsteadiness could first be perceived by eye. In each of these cases the collapse occurred after the first peak in net amplitude of 'steady' oscillation and was followed by a period of disordered oscillation which waned before suffering further agitation, the cycle being repeated indefinitely but with lessening variation in peak amplitude. Apparently the disorder is 'greater' in the longer than the shorter column.

From these figures, and recalling that the amplitude is presented logarithmically, a decaying modulation of oscillation is noted. Furthermore, in some cases as for trace 4, beats can be identified in the modulation itself. The traces naturally suggest the initial stages of damped forced oscillation. The time scale for the decay of initial modes of free oscillation is expected to be $(a^2/\nu\Omega)^{\frac{1}{2}}$ or 11·1 sec, according satisfactorily with the observations.

The inviscid free modes of oscillation, appearing as the final bracketed terms in (1.8) are modulated by frequencies $(\gamma_m(s) - 1)$, $\gamma_m(s)$, the dominant modulation

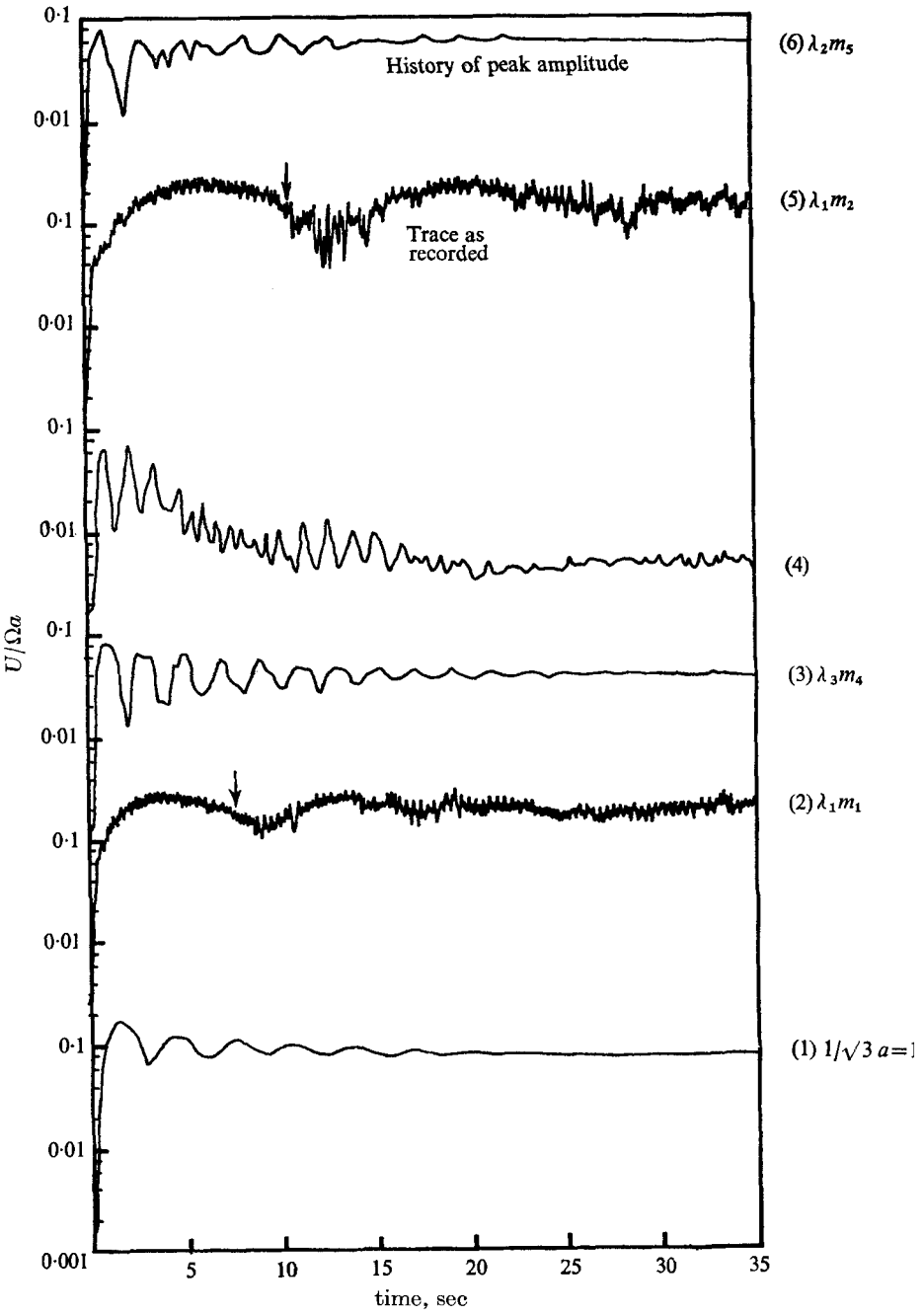

FIGURE 10. Amplitude of radial component of secondary oscillation. Measured by thermistor near axis, 1·3 cm above bottom of vessel, as a function of time after the introduction of a forcing disturbance, $\alpha = 0{\cdot}0342$, $R = 3{\cdot}48 \times 10^4$. Traces 1, 3, 4, 6, net peak amplitude; traces 2, 5, complete record. Arrows mark start of collapse. Successive traces displaced two decades.

being due to the simplest mode oscillation $\gamma_m(1)$; thus the beating period of the initial oscillation is

$$T_B = \frac{2\pi}{\Omega(\gamma-1)} = \frac{2\pi((\lambda_1/a)^2+m^2\pi^2)^{\frac{1}{2}}}{\Omega(2m\pi-((\lambda_1/a)^2+m^2\pi^2)^{\frac{1}{2}})}. \tag{2.2}$$

For $\lambda_1 = 2{\cdot}734$, T_B is plotted in figure 11 against column length/radius ratio. The curves repeat themselves for integral multiples of the fundamental resonance length.

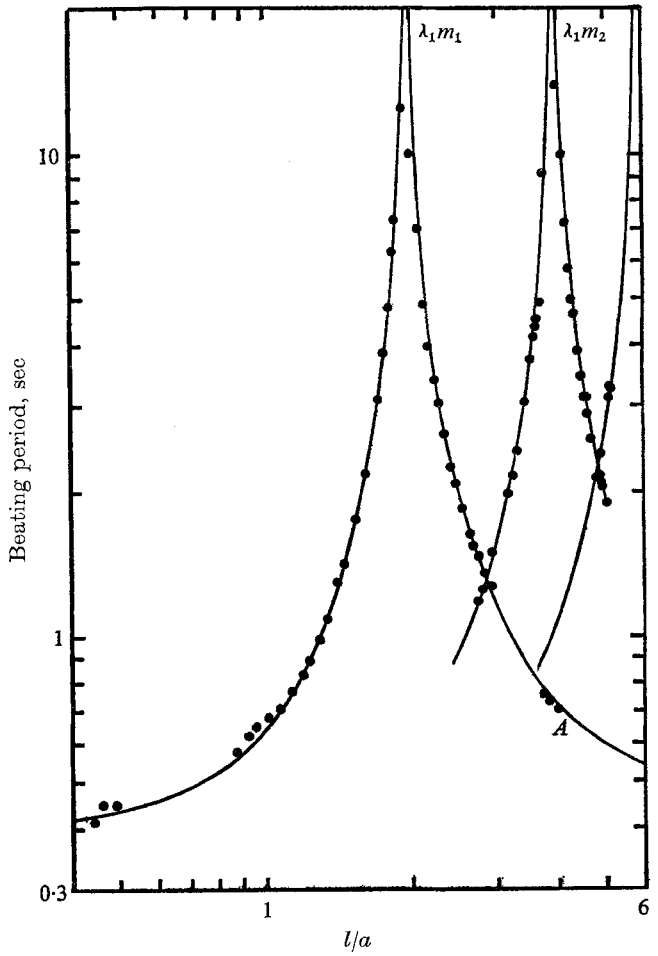

FIGURE 11. Initial periodic modulation of amplitude. Dependence on cylinder configuration. Theoretical curve gives the beating period of forced with free oscillation modes. ●, experiment; —, inviscid theory.

From the thermistor traces the amplitude modulation period could be measured directly and is plotted on the same figure. Where beating of the modulation occurred two separate periods could be defined and reveal on the figure crossover between successive harmonic forms of the first mode. Over the whole experimental range the agreement is remarkably good, and is regarded as substantial support for the inviscid definition of the simplest mode of free inertial oscillation.

2.3.2. *The amplitude–column height spectrum.* From a collection of records such as those in figure 10 the amplitude at the first peak and the 'final' amplitude was plotted against column height to give the spectrum shown in figure 12. For this plot $\alpha = 0{\cdot}0342$, $R = 3{\cdot}49 \times 10^4$. The experimental points are compared with the inviscid spectrum of summed modes λ_s from λ_1 to λ_5, with $\omega = 1$. Resonance of each mode is identified by a number. In drawing the spectrum, steps of 0·00866 in l/a were taken. Each downward cusp denotes a phase reversal, and a region of very low but finite amplitude is to be noted at l/a about 0·8 and 2·9. The curve is of *logarithm* modulus of radial velocity $U/\Omega a$ component at $z = 0{\cdot}27a$, $r = 0$, corresponding with the location of the thermistor. The experimental 'peak' spectrum is seen to respond principally to the lowest (λ_1) mode suggesting that its amplitude arises mainly from contributions of the initial free mode of this resonance. The 'final' spectrum likewise follows the lowest mode, and although responding to broad band departures from this mode, does not generally reveal the higher resonances to any appreciable degree. There is a marked response in this spectrum to the two very low amplitude regions.

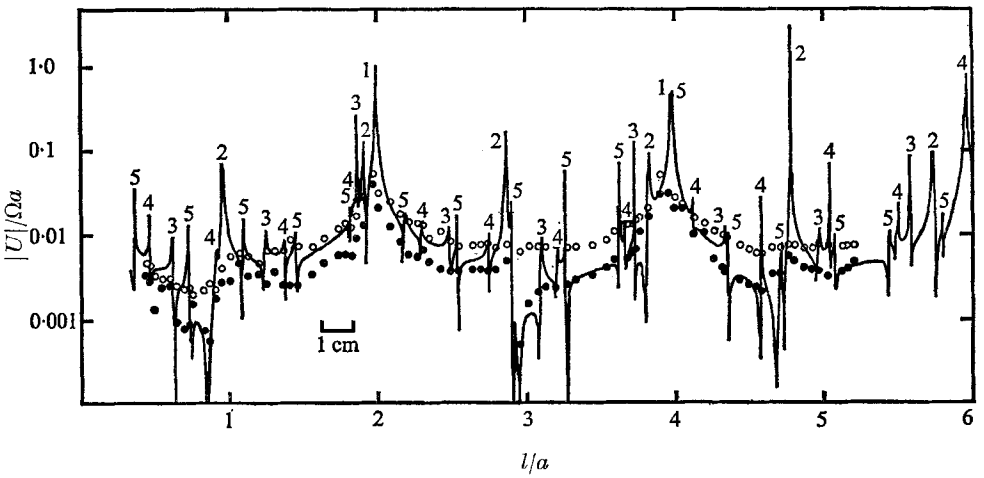

FIGURE 12. Amplitude–column height spectrum. Derived from measurements of radial velocity at a position $r = 0{\cdot}038a$, $z = 0{\cdot}27a$; $R = 3{\cdot}5 \times 10^4$; $\alpha = 0{\cdot}0342$. Column height stationary. Amplitudes are of first peak (before collapse) and after decay of initial modes. ○, peak amplitude; ●, final amplitude; —, inviscid theory.

2.3.2.1. *'Continuous' spectra.* To avoid the prohibitive amount of labour involved in filling in the detail of the experimental spectrum the apparatus was modified in the following way to make the acquisition of data a semi-automatic process. The axial rod (see figure 1) was threaded and the collar was replaced by a threaded bore spur gear. On the cross-head was mounted a component planetary gear meshing with this and another coaxial gear fitted to the radial arm, to complete an epicyclic system giving a large reduction in nut speed from the basic rotation rate. The rod itself also engaged the pin through another radial arm so that as the cylinder turned the rod was raised (or lowered by reversing the direction of rotation) on the threaded gear. The dimensionless rate of rise or descent $|\dot{l}|/\Omega a$ was $2{\cdot}06 \times 10^{-4}$ and the top position was monitored electrically.

Figure 13 compares representative spectra obtained with an ascending (dashed) and descending (dotted) top, against the inviscid spectrum. As before $\alpha = 0{\cdot}0342$; the Reynolds number was slightly higher ($5{\cdot}2 \times 10^4$). Again the broad features of the spectrum are followed, most particularly the nodes at $l/a = 0{\cdot}8$, $2{\cdot}9$ and the lowest under oscillation mode, but, although local peaks do occur in almost precisely the correct places, the response to higher mode resonances is indefinite. The apparent difference in the spectra on ascent and descent of the λ peaks is largely a result of resonant collapse which for both the ascending and descending top results, persisted after the first attainment of peak amplitude. In each case, this peak was displaced leftwards from the inviscid resonance position.

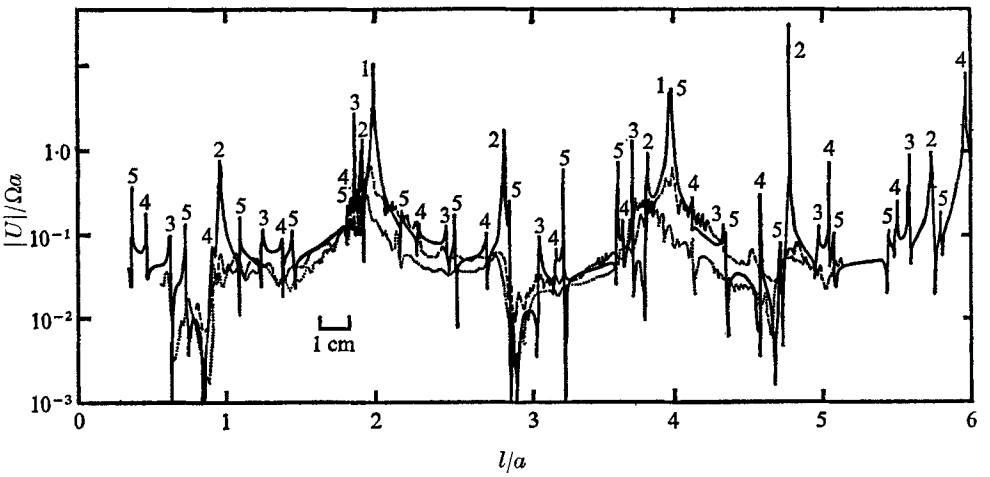

FIGURE 13. Amplitude–column height spectrum obtained with top ascending or descending at rate $2{\cdot}06 \times 10^{-4}\,\Omega a$. $\alpha = 0{\cdot}0342$; $R = 5{\cdot}2 \times 10^4$. —, inviscid spectrum, λ_1 to λ_5 modes; – – –, ascending top; ..., descending top.

The poor resolution of spectrum detail in the experimental curves appears to be due partly to the inability of the oscillation to undergo the rapid changes in phase which accompany each resonance, or to respond to the extremely narrow nodes of amplitude adjacent to these peaks. For much of the spectrum, the oscillation was 'disordered' to a degree by resonant collapse, which also obscured the individual resonant peaks. The fractional change in column height occurring during the viscous decay of a given mode is of order $2{\cdot}06 \times 10^{-4} \times R^{\frac{1}{2}} = 0{\cdot}047$. This 'bandwidth', though not inordinately large, is sufficient to encompass most of the spectrum detail.

Spectra for weak and strong excitation at high and low Reynolds number were also obtained but are presented elsewhere (McEwan 1968). At low Reynolds number further fine scale detail is lost in the spectrum but nodal positions and resonances remain near the theoretical locations. For high Reynolds number the peaks in the spectrum are truncated by resonant collapse. Nodal positions are shifted positively in l/a and resonant peaks *before* collapse are shifted negatively in l/a as for the spectra in figures 12 and 13. Higher mode resonances are revealed more clearly.

3. Viscous and finite amplitude effects

Till now attention has been directed mainly to establishing how closely the experimentally observed behaviour accords with *inviscid* theoretical predictions. With a finite Reynolds number some of what was observed might have been expected intuitively; in particular, since for secondary oscillatory motion the viscous diffusion length scale is at least $O((\nu/\Omega)^{\frac{1}{2}})$, modes s of order $R^{\frac{1}{2}}$ and greater must be modified and are probably suppressed by viscous action. Wood's (1966) analysis establishes that the viscous 'cutoff' occurs for modes above $s = O(R^{\frac{1}{3}})$ so that the internal discontinuities, which cannot be sharper than the spatial periodicity of the components forming them, have thickness of order $R^{-\frac{1}{3}}$. So far as they go, the present results have confirmed this. A second direct effect of viscosity to be anticipated is a change in oscillation induced by wall layers. Viscosity confers upon the roots for the boundary condition of the interior motion $u(a) = 0$, imaginary components of order R^{-1}, thus changing by the same order the column proportions for resonance. One primary effect of these motions is a modification to the ratio of forcing and rotation frequencies, and, if it is supposed that the effect on this ratio is of the same order as the viscous modification itself, then the magnitude of the change in resonant column height can be estimated directly:

$$\Delta(l/a) = O\left(\alpha R^{-\frac{1}{2}}\left[\frac{\partial(l/a)}{\partial\sigma}\right]\Omega_{\lambda,\sigma=\Omega}\right) = O(\alpha R^{-\frac{1}{2}}), \tag{3.1}$$

which, except in the case of intense resonance, would, nevertheless, be imperceptibly small. It is not surprising, therefore, that the calculated and observed resonances correspond in position as well as they do. It will be seen, however, that finite amplitude effects arising in resonances of the lowest mode, are capable of an appreciable influence on the effective rotation frequency, and hence on the resonant column height.

The peak amplitude of this mode at resonance is not linearly dependent on rotation rate, and this is sufficient evidence that the amplitude is controlled to some degree by viscosity; but neither is the amplitude small compared with $R^{-\frac{1}{2}}$, so that the non-linear terms in the momentum equation assume an importance in describing the flow field.

In the following pages, the magnitudes of *linear* viscous constraints are first predicted and found to be inadequate in defining the limits to the oscillation when the forcing disturbance is not small.

The sizes of the largest non-linear contributions are estimated and their presence is demonstrated in a simple experiment. An interpretation of their influence on the main oscillation field leads to a model describing the acquisition of energy by the secondary motion which compares favourably with the experimental observations.

3.1. *Mechanisms controlling the amplitude of resonant oscillation and further experiments*

3.1.1. *Observations of phase shift and amplitude evolution.* In the absence of viscosity, a resonant oscillation can acquire energy from the net rotation only

by the action of those components of the pressure field at the plane of the top in anti-phase with the top slope, $\alpha \cos\phi$. The velocity field must have corresponding components in order that core patterns visible in the plane $\phi = 0$ (figure 2) be explained.

Referring to (1.8), in addition to weak resonant and non-resonant initial modes (terms III, IV, V, VI, VII), is the main resonant growth mode (II), which increases linearly with time. That these modes by themselves are ineffective in describing the secondary field for times $n \gg 1$ can be inferred by plotting the thermistor bridge output in lissajou form against $\sin\phi$. Figure 14 presents the histories of

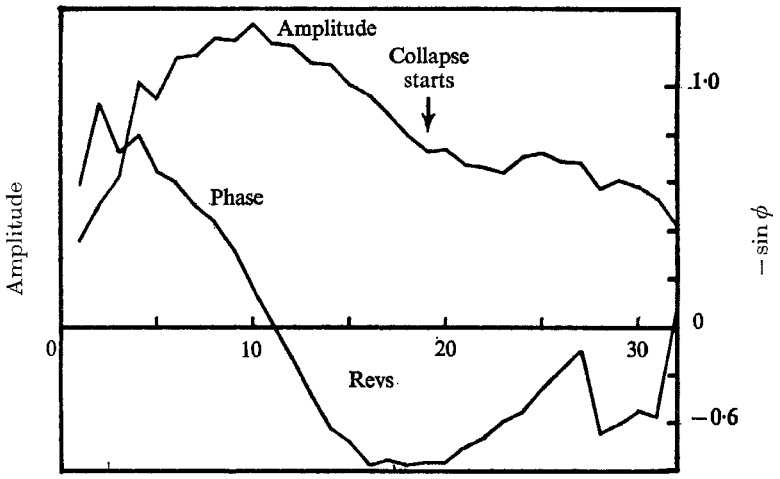

FIGURE 14. Amplitude and phase history of resonant oscillation. $\lambda_1 m_2$ mode, $R = 0{\cdot}88 \times 10^4$, $\alpha = 0{\cdot}0702$. Phase is shown of peak in amplitude U relative to top $z = l + \alpha r \sin\phi$.

peak amplitude $U = |u|/\Omega a$ and phase till resonant collapse for the $\lambda_1 m_2$ mode, $\Omega = 4{\cdot}25$ rad/sec, $\alpha = 0{\cdot}0702$. Since according to the linear field description the perturbation pressure is proportional to oscillation amplitude, the product of the two curves will represent the power extracted from the top in exciting the resonant mode. Notably, the peak amplitude occurs immediately before the oscillation reaches a position with zero antiphase component.

In contrast, by (1.11) the theoretical phase of peak velocity rises, with a rapidly decreasing modulation of frequency $2n$, to within arsin $(-0{\cdot}99)$ in less than one container revolution. The 'initial value' linear solution ((1.8)–(1.11)) is thus evidently unrealistic for the present purpose.

The experimentally observed phase shift was monotonically *prograde*, i.e. in the direction of rotation, the peak positive radial amplitude increasing in phase from the third quadrant in ϕ.

Unsteady oscillations preceding collapse appeared after 19 revolutions but do not seem from figure 14 to be associated to any marked degree with a *change* in phase or amplitude (or energy transfer). Collapse was complete at 24 revolutions, after which phase changes were too rapid ($O(\Omega)$) to be identified with oscillation amplitude. The mean phase shift remained small after collapse.

3.1.2. *Viscous amplitude control: linear magnitudes.* Thus far there are no

direct indications of *how* the self control of phase is brought about in the evolution of the oscillation, and it is appropriate first to examine the magnitude of predictable viscous effects. From Wood's (1966) linearized viscous analysis the constraint arising from the appearance of non-vanishing imaginary terms in the denominator of (1.2) and representing dissipation in the interior motion (cf. Wood's (7.4), (3.1), (2.14)) is only $O(R^{-1})$ and is quite insufficient to produce the observable differences between the high and low Reynolds number spectra, let alone the *control* of amplitude. Wood estimated the magnitude of the internal velocities and shears near to the characteristic for non-resonant column lengths, concluding that the magnitude of the modification to the inviscid field was derived from the summation of individual modes $O(R^{\frac{1}{3}})$ in number, each possessing a magnitude $O(R^{-\frac{1}{2}})$ the cumulative value being $O(R^{-\frac{1}{6}})$.† Tempting though it is to seek constraints having this order of magnitude, these results cannot be regarded as pertinent when applied to individual free modes.

The dissipation within the viscous wall layers owing to the relative movement of free oscillation of amplitude $\mathbf{q}$ is $O(\mu|q|^2R^{\frac{1}{2}}a)$, μ being viscosity, while the power available from the top in the presence of the interior velocity field is $O(\rho\Omega^2\alpha qa^4)$ so long as the secondary pressure field $O(\rho\alpha\Omega qa)$ remains in antiphase with the top slope. Equating these gives an upper limit to the amplitude

$$q/\Omega a \ll O(R^{\frac{1}{2}}\alpha). \tag{3.2}$$

This is evidently a realistic description provided the amplitude is small, but in the range of parameters of the present experiments viscosity gains effectiveness only in motions greater than the basic rotation.

If we persevere with the notion that a truly steady state *is possible* then recognizing phase control as the physical amplitude regulating mechanism we have to suppose that the true averaged phase shift in the absence of viscosity would be zero, and propose that viscosity induces motion which if unsymmetrical might result in a secondary antiphase pressure field at the top to counter boundary dissipation. The highest-order contribution to such a field is $O(\rho\alpha\Omega qaR^{-\frac{1}{2}})$, so that the 'steady state' oscillation amplitude is stabilized at a magnitude $O(R^{-\frac{1}{2}})$ of that given in (3.2), i.e.

$$q/\Omega a = O(\alpha), \tag{3.3}$$

if, as was assumed before, most of the dissipation takes place in layers $O(R^{-\frac{1}{2}})$ thick.

Equations (3.2) and (3.3) would then be regarded as the asymptotic limits to $q/\Omega a$ with low α at low and high Reynolds numbers respectively. In this case, however, the oscillation would under no condition be much larger than the forcing amplitude itself, a situation not supported by observations of resonant peaks typically an order of magnitude greater (and evidently truncated by collapse rather than by viscosity).

3.1.3. *Azimuthal circulation.* For $q < R^{-\frac{1}{2}}$ the non-linear terms $O(q^2/\Omega)$ neglected from the momentum equation (1.1), assume a magnitude comparable

† Wood's result applies provided $O(R^{-\frac{1}{6}})$ terms are dominant over those $O(R^{-\frac{1}{3}}\ln R)$ which also appear. On an experimental scale these are of the same order but the conclusion is not seriously jeopardized.

with those of viscosity. If the formal description of the flow relative to the boundaries as given by (1.2) were retained, it is likely that the tertiary field would also be symmetrical in ϕ. The real situation, however, is one in which the main oscillation *grows* after the introduction of the forcing disturbance and thereafter must be sustained against viscosity. The cylinder walls and bottom are ϕ independent, so that in an inviscid fluid the normal stress at these boundaries could not transmit to the cylinder walls, the axial component of the couple generated by the secondary pressure field acting on the sloping top surface. Thus the secondary motion must be initially created *at the expense* of the primary rotational energy. Writing $\Delta\Omega$ as the scale of the loss in angular velocity (a net azimuthal, i.e. retrograde, westwards motion imposed on the original rotation),

$$\Delta\Omega = O(q^2/\Omega a^2), \tag{3.4}$$

with no change in total kinetic energy, if $q \gg \alpha\Omega a$.

In a steady-state oscillation most energy is dissipated at the walls in layers $O(R^{-\frac{1}{2}}a)$ thick, at a rate $O(\mu q^2 a R^{\frac{1}{2}})$ for the whole container. To extract power the cylinder drive at this rate, the azimuthal component of the tertiary motion must be capable of producing a tangential shear stress $O(\mu q^2 R^{\frac{1}{2}}/\Omega a^2)$. If the thickness scale of the azimuthal component of the wall boundary layers is also $O(R^{-\frac{1}{2}}a)$ then, as before,

$$\Delta\Omega = O(q^2/\Omega a^2).$$

In both generation and steady-state conditions, therefore, the tertiary motion should contain an azimuthal *component* of the same order of magnitude.

The presence of this motion was confirmed experimentally by mounting in the cylinder an axial needle, on the end of which was balanced a light free turning wire cross 8·5 cm in diameter resting in the plane $z = \frac{1}{2}$. With the cylinder in the resonance configuration, the rate of rotation of the cross was monitored using a strobo-tachometer and pen recorder for a period following the introduction of the forcing disturbance. Typically, the cross relative to the container assumed within a few revolutions a more or less constant westward rotation, which although slightly unsteady after resonant collapse, maintained the same magnitude, as well as could be judged by the simple monitoring procedure.

Figure 15 shows the results of westward drift $\Delta\Omega$ averaged over 40 revolutions commencing about ten revolutions after arresting the top frame, for top slopes of 0·035 and 0·070. In each case, the leftmost point represents the lowest Reynolds number at which the drift could be measured. At less than this there seemed to be an abrupt drop in $\Delta\Omega$ below the trend of points, to an almost unmeasurable level. This observation is significant as will be seen.

The results are compared with the observed dependence of peak amplitude before resonance on Reynolds number (presented in figure 17) obtained from amplitude evolution traces like figure 10. Each of the solid lines on figure 15 represents the square of the amplitude $(U/\Omega a)$ at the appropriate value of α, taking the functional dependence to be a power of Reynolds number over the relevant range. A common factor of 0·48 brings these lines to agreement with the observed azimuthal drift, which therefore appears to possess the dependence on

oscillation amplitude given by (3.4), notwithstanding the fact that this amplitude did *not* remain steady.

The preceding technique was unsuitable for measurement of the azimuthal motion during the initial stages of evolution, and no simple means could be devised for monitoring the motion continuously. To give a crude indication of the radially averaged motion in these stages, the following method was employed.

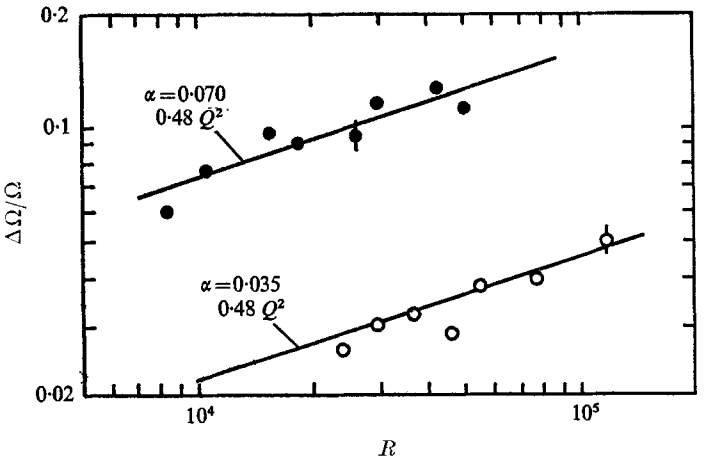

FIGURE 15. Westward azimuthal circulation $\Delta\Omega$ relative to basic rotation. Measured in plane $z = \frac{1}{2}l$. $\lambda_1 m_2$ resonant mode. Comparison with square of oscillation amplitude Q.

The stroboscopic lamp was flashed synchronously with the container rotation and the position of the cross-wire in relation to the container was observed in the light of each flash. By timing the arresting pin engagement to coincide with the flashes, it was possible to estimate within one half a container revolution, the number of revolutions elapsing from the cross to execute $\frac{1}{4}$ turn, $\frac{1}{2}$ turn, etc., relative to the container.

Observations were made with the cross in the planes $z = 0{\cdot}27a$, $1{\cdot}0a$ and $1{\cdot}99a$; the number of container revolutions observed for a convection of one quarter-turn was found to be reproducible within about one revolution.

Tabulated below are the results at various Reynolds numbers with a forcing disturbance of 0·0344. The container revolutions for one-quarter of a revolution, and one-half a revolution of the cross are given. The convection in planes $z = 0{\cdot}27a$ and $1{\cdot}99a$ are similar, as one might expect from the symmetry of the oscillation field, and both are significantly greater than in the intermediate plane; while in the former planes, however, the convection rate diminished more or less continuously with decreasing Reynolds number, in the intermediate plane it varied in an irregular fashion. During the evolution the cross in this plane would dwell in position and sometimes *reverse* its direction of motion during the first half-cycle. In practically all observations in the $z/a = 0{\cdot}27$ and $z/a = 1{\cdot}99$ planes immediately after the introduction of the disturbance there was a small (about 20°) *prograde* motion of the cross.

Unless α is very small indeed the azimuthal circulation is a good deal greater than the $O(\alpha R^{-\frac{1}{2}})$ Ekman induced motion which led to the estimate of change in column height given in (3.1). An equation of the same form,

$$\Delta(l/a)_{\text{resonant}} = [d(l/a)/d\omega]_{\lambda_1 \text{ mode}} (d\omega/d\overline{\Delta\Omega})\,\overline{\Delta\Omega} + \ldots \quad (\omega = 1),$$

indicates the change in resonant column height to be expected from this motion.

Plane	$z = 0{\cdot}27a$		$z = a$		$z = 1{\cdot}99a$		Mean N for $-\Delta\psi = \frac{1}{2}\pi$ (theory)
	$-\Delta\psi = \frac{1}{2}\pi$	π	$\frac{1}{2}\pi$	π	$\frac{1}{2}\pi$	π	
$R \times 10^{-4}$	Number of container revolutions elapsed for $-\Delta\psi$ retrograde zonal convection						
5·86	10	15	24·4	54·3†	11·3	14·9	17·5
3·72	13	16	18·5	29·5‡	10·5	15·0	18·0
2·60	13	16·5	18·5	26	12	16	19·1
1·64	15	18·5	18·0	26	14	18	21·0
0·79	18·5	24	58·0§	70	17	24	25·4
0·605	23	34	30·5	49	22	40	27·8

$\Delta\psi$ is the retrograde change in phase from the initial position of the cross.

† The cross reverted almost completely to $\Delta\psi = 0$ before returning to the $\Delta\psi = \frac{1}{2}\pi$ position.

‡ Long hesitation in this position.

§ No movement from $\Delta\psi = 0$ for 50 revolutions.

The final column is explained in §3.1.4.1.

TABLE 3. Measured container revolutions for $\frac{1}{4}$ and $\frac{1}{2}$ turn retrograde relative motion of cross

		$\Delta l/ma$			
α	$R \times 10^4$	Estimated		Measured	
0·170	0·8	−0·007	−0·005	+0·01	−0·01
	4·3	−0·016	−0·010	0	—
	5·2	−0·016	−0·012	0	—
0·0342	3·5	−0·057	−0·031	−0·03	−0·05
0·0684	5·2	−0·071	−0·041	−0·05	−0·03
0·0684	0·8	−0·077	−0·077	−0·12	−0·10
	5·2	−0·134	−0·095	−0·20†	—

† Resonant collapse obscures amplitude peak.

TABLE 4. Shift in column height for peak resonance amplitude λ_1 mode due to finite amplitude effects

The first derivative has a magnitude +2·30 m for λ_1 inviscid resonance. The second derivative, representing the dependence of the ratio of rotation frequency to the 'net' disturbance frequency on the tertiary field (whose scale of azimuthal motion is $\overline{\Delta\Omega}$), is not defined with such certainty, since its value apparently depends on the non-uniform distribution of vorticity in the tertiary motion. If the net rotation rate changed to $\Omega - \overline{\Delta\Omega}$ without a proportionate change in free oscillation frequency from $\sigma = \Omega$ the derivative would have the value −1, in which case most intense resonance would occur at a column somewhat shorter

than the theoretical. This is the case in practice. Tabulated above (table 4) are the observed shifts in l/a for peak oscillation of the mode *before collapse* from the amplitude height spectra with ascending cylinder top. Compared with these is $\Delta l/ma$ calculated from the above equation with $(d\omega/d\overline{\Delta\Omega}) = -1$, $\overline{\Delta\Omega}$ being given theoretically (by (3.11)) by energy conservation considerations. Agreement is fair both in sign and magnitude.

3.1.4. *Physical mechanisms for the generation and regulation of resonant oscillation.* It has been established that viscosity is not necessarily effective in limiting the amplitude of resonant oscillation. Further, it was noted that after very short times the linear initial value analysis is ineffective to describe the evolution of the oscillation, but that there existed a possible association between the phase of the oscillation and its rate of growth.

From the remarks of the previous subsection, the impulse on the fluid by the top to create the oscillation results in an azimuthal motion persisting for a time at least $O(R^{\frac{1}{2}})$, and it is reasonable to associate the phase change of the oscillation with the azimuthal motion over this time. Therefore, the oscillation might be considered as commencing from an initial phase position given by the linear growth term (II) in (1.8) (i.e. the pressure in antiphase to the slope in the plane of the top), and, after a dimensionless time of order unity, as growing at a rate defined by its own phase relative to the top. Such behaviour is physically equivalent to that of a nearly resonant free mode; however for large beating periods T_B (equation (2.2)), such a free mode will energize itself to an extent where the resultant motion affects the field description, i.e. $T_B \geqslant \overline{\Delta\Omega}^{-1}$. The ratio of rotation and natural frequency of an intense oscillation must be changed by an amount depending upon the azimuthal drift rate $\overline{\Delta\Omega}$, and the evidence of table 4 and the leftward shift of beating period near resonance in figure 11, suggest that the frequency ratio is changed by roughly the same magnitude as the retrograde azimuthal drift, i.e.

$$\Delta\omega \sim \overline{\Delta\Omega}/\Omega.$$

3.1.4.1. *Integral energy analysis for finite amplitude evolution.* It is instructive now to formulate an approximate equation representing an energy balance between the rate of gain in kinetic energy of the free mode, the impulse provided by the top and the viscous dissipation. If Q is a characteristic magnitude, taken for the present purpose as $U_t/\Omega a$ (U_t here being the peak amplitude at the thermistor position $z = 0{\cdot}27a$), and the main oscillatory mode is supposed to retain a similar *form* independent of amplitude, then, ignoring temporal derivatives to the linear approximation of (1.1), the pressure field on the top surface also retains similarity, has a magnitude proportional to Q, and imposes a couple, which to first order has an axial component,

$$T = \int^{a}\int^{2\pi} P(r, \phi, \psi)\,\alpha\cos\phi\, r^2\, dr\, d\phi, \tag{3.5}$$

on the top surface lying in the plane $z = l + \alpha(r/a)\sin\phi$. ψ is the angle in the ϕ direction, by which the peak pressure *leads* the plane $\phi = \pi$ (i.e. the reduced pressure field has the form $-P(r, z)\cos(\phi - \psi)$. Superimposed on the pressure field of the resonant mode is that of forced and free non-resonant modes, terms

I, VI and VII in (1.8), and free steady resonant modes, terms III, IV and V. These exert no average torque on the top, and it is further assumed that viscosity-induced tertiary modes created by these modes are insignificant.

We now consider the evolution of the lowest (λ_1) mode of resonant oscillation. The linear inviscid *form* of the pressure field is taken to hold for finite amplitudes; thus it is noted that from (1.2) and (1.3), or (1.8) and (1.11), that

$$P = 3aJ_1(r')\,Q\cos(\phi-\psi)/(\cos(0{\cdot}27\lambda_1/\sqrt{3})\,[J_1'(r')+2J_1(r')/r']_{r'=0},$$

and

$$T(\psi) = \frac{2\rho\Omega^2a^5\pi Q\alpha\cos\psi}{\lambda_1^4\cos(0{\cdot}27\lambda_1/\sqrt{3})}\int_0^{\lambda_1} r'^2J_1(r')\,dr' \tag{3.6}$$

with $\psi(t=0)=0$, $\sigma=\Omega$. Here $\lambda_1 = 2{\cdot}73462$, the first positive root of (1.2) for $\omega = 1$; $r' = \lambda_1 r/a$.

Before the momentum transferred by viscosity at the walls of the container becomes significant (i.e. before the retrograde circulation has caused an internal convection field to be induced by Ekman layer entrainment), the torque at the top plane must equal the rate of change of angular momentum of the whole fluid cylinder; if $\overline{\Delta\Omega}$ is the *mean* loss in angular velocity

$$\frac{d\,\overline{\Delta\Omega}}{d\tau} = 2T/\rho\pi la^4. \tag{3.7}$$

With negligible dissipation in the *bulk* of the fluid, kinetic energy is conserved, so neglecting the energy in the azimuthal motion itself,

$$\frac{l\pi a^4}{2}\,\Omega\,\overline{\Delta\Omega} = \int^V \frac{q^2}{2}\,dV;$$

q is the total disturbance velocity, and contains the forced modes as well as the resonant free mode, V is the volume. After $O(\Omega^{-1})$ in time, the last becomes dominant, but the impulse required to establish the forced modes will have contributed to the retrograde convection an amount $O(\alpha^2\Omega)$. The magnitude of the integral can be estimated from the field description of (1.2) and (1.3) for the λ_1 mode, giving

$$\overline{\Delta\Omega} = \frac{2\Omega Q^2}{9\cos^2(0{\cdot}27\lambda_1/\sqrt{3})\,\lambda_1^2}\left\{\int_0^{\lambda}\left[5J_0^2(r') - \frac{2J_0(r')\,J_1(r')}{r'} + 2\left(\frac{J_1(r')}{r'}\right)^2 + 3J_1^2(r')\right]r'\,dr'\right\} + O(\alpha\Omega Q) + O(\alpha^2\Omega). \tag{3.8}$$

From above with I_1 and I_2, the value of the integrals in (3.6) and (3.8)

$$\frac{dQ}{dn} = \frac{a}{l}\,\frac{9\cos(0{\cdot}27\lambda_1/\sqrt{3})\,I_1\alpha\cos\psi}{\lambda_1^2 I_2}. \tag{3.9}$$

By numerical integration $I_1 = 3{\cdot}5346$, $I_2 = 6{\cdot}6667$. Then for the $\lambda_1 m_2$ free mode at resonance ($l = 3{\cdot}992a$) with $\Omega = \sigma$ in the absence of dissipation

$$dQ/dn = 0{\cdot}145\alpha\cos\psi, \tag{3.10}$$

$$\overline{\Delta\Omega}/\Omega = 0{\cdot}239(Q+O(\alpha))^2. \tag{3.11}$$

If the modes were truly independent of one another the first equation would apply after the impulsive creation of non-resonant modes; thereafter each mode would be associated with its own pressure field. These modes, however, make the contributions on the right of (3.11). Using the steady-state field description as before, the terms were evaluated for modes λ_2 to λ_5. For λ_1 resonance these contributions are found by computation to be insignificant in the early stages of evolution.

A third significant term in the energy balance is viscous dissipation. As mentioned earlier the wall boundary-layer dissipation is dominant. Fluid particles in the inviscid core adjacent to the walls describe elliptical tangential paths, and it would appear that a fair approximation for the boundary-layer dissipation is had by ignoring the contributions due to the non-uniformity of this tangential motion. Also ignored are rotational effects, though these at least could be calculated. For the present purpose the main effect of such terms is a small change in the numeric factor.

To first order then, Stokes's classical periodic boundary-layer description is applicable, with superimposed orthogonal periodic velocities; for the flow near the top and bottom surfaces

$$q = U[\cos n - e^{-\eta}\cos(n-\eta) + V\{\sin n - e^{-\eta}\sin(n-\eta)] \tag{3.12}$$

$\eta = \hat{N}\sqrt{(\Omega/2\nu)}$, $\hat{N}$ being an inward surface normal. The expression for motion $q(V, W, \eta)$ near the side walls is similar.

Over unit surface area the energy dissipated through the layer in one cycle ($n = 2\pi$) is

$$\frac{\rho(U^2+V^2)}{2}\left(\frac{\nu}{\Omega}\right)^{\frac{1}{2}}\pi\sqrt{2}.$$

The same cyclic variation in q is experienced over all elements of a circular area of the top or bottom, so that the dissipation on each surface in the time elapsed for one radian of container revolution is

$$\frac{\rho\pi\sqrt{2}}{2}\left(\frac{\nu}{\Omega}\right)^{\frac{1}{2}}\int_0^a [U^2(r,0)+V^2(r,0)]\,r\,dr$$

$$= \frac{\rho\sqrt{2}}{2}\frac{4}{9}\frac{Q^2R^{-\frac{1}{2}}}{\cos^2(0{\cdot}27\lambda_1/\sqrt{3})}\frac{a^3}{\lambda_1^2}\int_0^\lambda [5J_0^2r' - 2J_0J_1 + 2J_1^2(r')]\,dr'. \tag{3.13}$$

The value of the integral being 3·752 for $\lambda = \lambda_1 = 2{\cdot}734$. A similar expression is derived for the cylinder wall layer. For a single module of the lowest λ_1 mode, the dissipation/radian is

$$\frac{\rho\sqrt{6}}{2}\frac{\pi^2 4}{9}\frac{Q^2R^{-\frac{1}{2}}}{\cos^2(0{\cdot}27\lambda_1/\sqrt{3})}\frac{a^3}{\lambda_1}\left\{\left(2J_0(\lambda)-\frac{J_1(\lambda)}{\lambda}\right)^2+3J_1^2(\lambda)\right\}; \tag{3.14}$$

the value of the bracketed quality for $\lambda = \lambda_1 = 2{\cdot}734$ is 0·7712.

Notwithstanding the obscurity of the association between the azimuthal component of the tertiary field (which appears as change in net angular velocity), and rate of phase change of the free oscillation relative to a stationary observer, it is postulated that the azimuthal motion is the only modification to the flow

possessing sufficient magnitude to produce this phase change. Accordingly we now examine the consequences of a direct linear connexion between the phase change rate and the loss of net angular velocity.

Thus, if the pressure field is convected 'intact' at the *mean* azimuthal circulation rate, but in an opposite direction,

$$\overline{\Omega}\frac{d\psi}{d\tau} = \frac{d\psi}{dn} = \frac{\Delta\overline{\Omega}}{\Omega}.$$

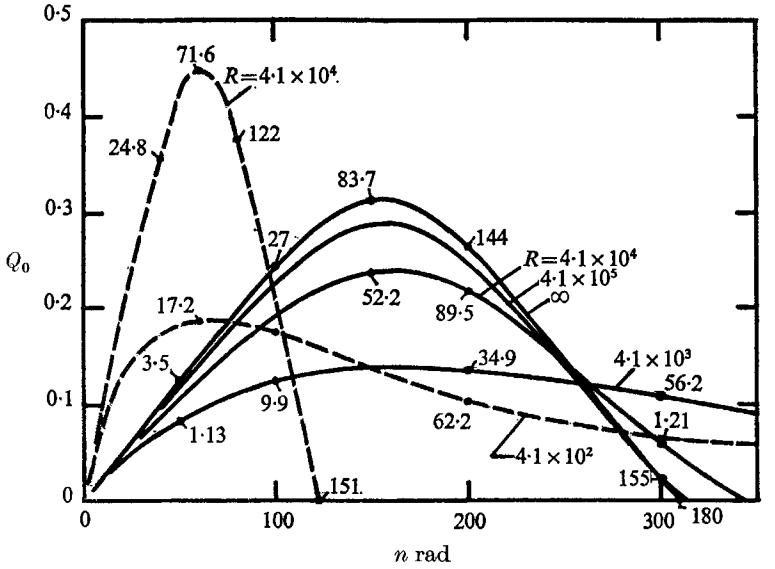

FIGURE 16. Solution of integral energy equation for resonant oscillation of $\lambda_1 m_2$ mode. Dimensionless amplitude Q_0, at $z = 0{\cdot}27a$, $r = 0$ *versus* dimensionless time. ——, $\alpha = 0{\cdot}0170$; – – –, $\alpha = 0{\cdot}0687$. Numbers give phase shift in degrees from initial position $\psi = 0$.

Starting from an initial position with no 'steady-state' component,

$$\psi = \int_0 \frac{\overline{\Delta\Omega}}{\Omega} dn = 0 \quad \text{at} \quad n = 0, \quad Q = 0,$$

and combining (3.10), (3.11), (3.13) and (3.14) in the form of an energy balance for the rotating fluid system (the last two equations being brought to dimensional consistency with the first), then, neglecting the smaller terms in (3.11),

$$\frac{dQ}{dn} = 0{\cdot}145\alpha \cos\left(\int_0 0{\cdot}239\, Q^2 dn\right) - 1{\cdot}013 QR^{-\frac{1}{2}} \tag{3.15}$$

for the $\lambda_1 m_2$ mode at resonance, and

$$\frac{dQ}{dn} = 0{\cdot}290\alpha \cos\left(\int_0 0{\cdot}239\, Q^2 dn\right) - 1{\cdot}414 QR^{-\frac{1}{2}} \tag{3.16}$$

for the $\lambda_1 m_1$ mode.

These equations were solved numerically and figure 16 gives the typical forms for two α's at various Reynolds numbers. Depending on whether the viscous dissipation exceeds a critical amount, the amplitude Q, after rising to a peak

value either falls again to zero (beyond which the solution ceases to have meaning) or falls at a decreasing rate to approach zero asymptotically. The difference between the two types of solution is identified by the magnitude of $\cos\psi$. If this is able to become negative while the amplitude is finite (sufficient convection has occurred to permit the oscillation to attempt to feed energy *back into* the mean motion), then a quick return to zero is inevitable. If viscosity prevents $\cos\psi$ from

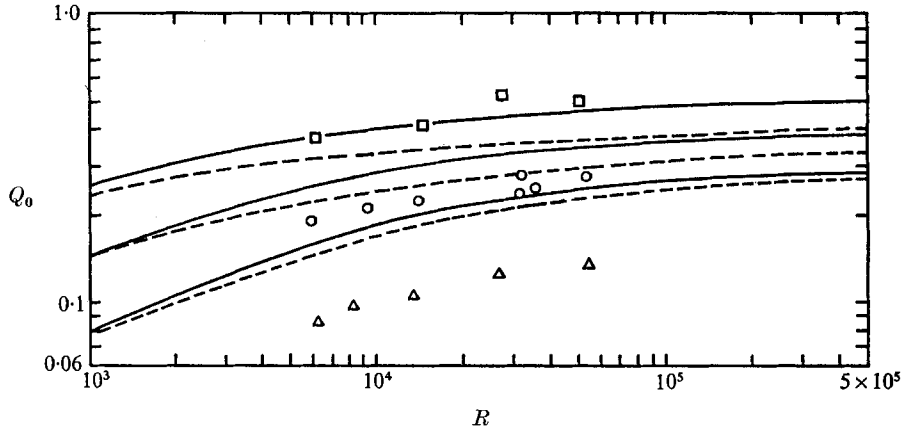

FIGURE 17. Theoretical and experimental peak amplitudes compared. $\lambda_1 m_2$ resonant mode. ——, resonant mode Q_0 only; – – –, net value, including λ_2 to λ_5 forced modes. □, $\alpha = 0{\cdot}0687$; ○, 0·0344; △, 0·0170.

falling to zero the oscillation continues to extract momentum from the top at an ever decreasing rate. One case $R = \infty$ is also presented, for which the curve is symmetrical, the peak occurring exactly at $\cos\psi = 0$. On the curves presented the numbers give the value of ψ in degrees at each point marked.

The solution is now examined in detail and compared with the observable properties of the amplitude traces obtained experimentally, of which figure 10(5) is a typical example. The comparison is not direct because the amplitude measured experimentally is not merely that of the resonant mode, but contains also the contributions from the forced higher-order modes, which combine *vectorially* with the resonant mode. The difficulty is that the phase of these contributions is unknown, and their amplitude is doubtless modified by viscosity. An upper limit to their influence can be gauged by assuming that they possess an amplitude and phase given by the inviscid theory, i.e. the radial amplitude at a point $z = 0{\cdot}27a$, $r = 0$, $\sigma = \Omega$ is

$$Q_{\text{non-resonant}} = \alpha 3\sqrt{3} \sum_{s=2} \frac{\cos(0{\cdot}27\lambda_s/\sqrt{3})\cos\phi}{(\lambda_s^2+3)J_1(\lambda_s)\sin(\lambda_s n\pi/\lambda_1)}, \tag{3.17}$$

for which, with summations to $s = 5$,

$$Q_{\text{n.r.}} = +1{\cdot}130\alpha\cos\phi, \quad \text{with the } \lambda_1 m_1 \text{ mode geometry,}$$

$$Q_{\text{n.r.}} = +1{\cdot}422\alpha\cos\phi, \quad \text{with the } \lambda_1 m_2 \text{ mode.}$$

Combined vectorially with the solution for Q given by (3.15) and (3.16), the net amplitude Q_N is lowered, slightly, and the value of ψ is increased. Figure 17

gives the peak amplitude for the $\lambda_1 m_2$ mode. The theoretical values of the forced mode alone (solid line) become dependent on half power of Reynolds number and directly proportional to α at low Reynolds number. The Reynolds number exponent diminishes continuously to zero and the amplitude becomes less dependent on forcing amplitude as the Reynolds number increases. The 'net' theoretical amplitude Q_N is shown as a broken line. For very low Reynolds number, the net amplitude does not follow the half-power relation, but asymptotes to the forced amplitude of the non-resonant modes.

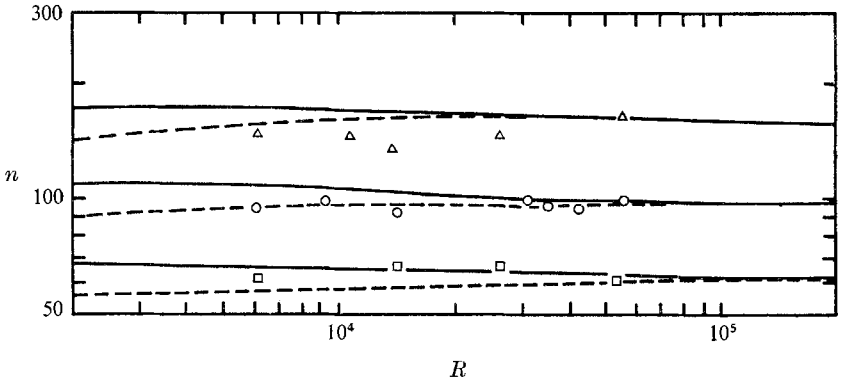

FIGURE 18. Dimensionless time to attainment of peak amplitude $\lambda_1 m_2$ resonance. ——, theory, resonant mode Q_0 only. – – –, theory, net oscillation, including λ_2 to λ_5 modes. □, α = 0·0687; ○, 0·0344; △, 0·0170.

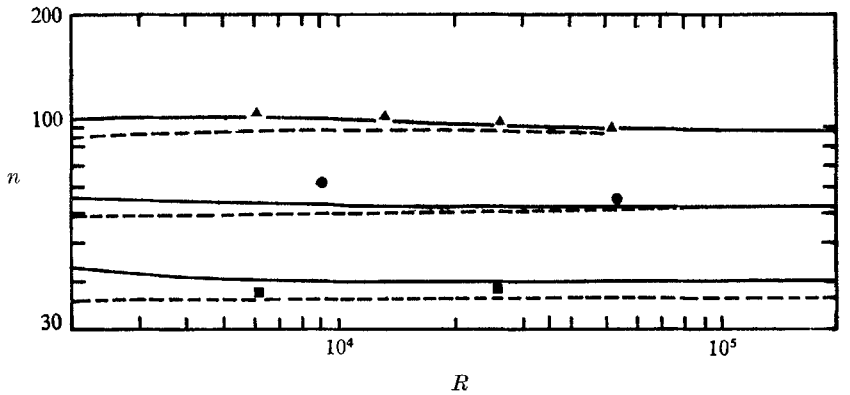

FIGURE 19. Dimensionless time to attainment of peak amplitude, $\lambda_1 m_1$ resonance. Legend otherwise as for figure 18. Symbols as for figure 18.

The experimental results suggest the correct dependence upon Reynolds number, but are more strongly affected by forcing amplitude. The correspondence of theory with experiment is best between α = 0·0687 and α = 0·0344, but the peak amplitude for lower α is progressively overestimated. Figures 18 and 19 compare the calculated and observed dimensionless time elapsed for attainment of the peak amplitude after starting the perturbation for $\lambda_1 m_2$ and $\lambda_1 m_1$ modes. As before the broken line indicates the time for the *net* oscillation to reach a maximum, which, because of the phase relation between the forced and free

modes, is less than that for the free oscillation *alone* (solid line) to reach its maximum.

Agreement of theory and experiment is close both in virtual independence of Reynolds number and in non-linear dependence upon α. The limit for vanishing viscosity is marked on the right-hand ordinate. Both solid and broken lines asymptote.

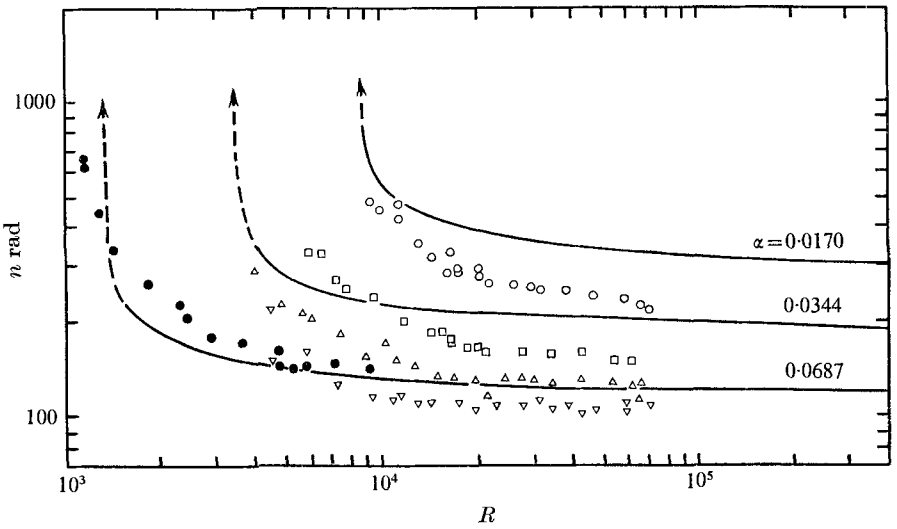

FIGURE 20. Observed dimensionless time to collapse, compared with theoretical time for a complete evolution cycle ($d\psi/dn = 0$, $Q_0 \to 0$). For Reynolds numbers below the leftmost point in each group, no resonant collapse was observed. KEY: open symbols as for figure 9, μ = 1·06 cp; ●, α = 0·0687, μ = 15·7 cp.

Figure 20 shows the dimensionless time for a complete evolutionary cycle during which, according to the theory, the amplitude has risen to a maximum and fallen again to that of the forced modes alone. From the infinite Reynolds number asymptote, the time rises abruptly as transition from subcritical to supercritical viscous dissipation is approached. For Reynolds number below the critical level, ψ does not reach $\frac{1}{2}\pi$ and the dimensionless time is infinite.

It is near this critical region that the α terms neglected from (3.11) for the zonal component of the tertiary motion assume an importance, since they provide azimuthal motion in the absence of free oscillation, and unless account is taken of energy supplied by 'spin-up' modes from the wall boundary layers, the abrupt transition to subcritical dissipation does not occur, though there is a sudden change in the gradient of the time line. Spin up would certainly neutralize the effect of the α terms for times $\gg R^{\frac{1}{2}}$, but is not easily quantified for inclusion in the present analysis.

Both in the approach to a constant cycle time at high R and in the existence of a lower limit in Reynolds number, the resemblance of the form of these curves to the observed revolutions (dimensionless time) to resonant collapse is at once apparent, and the results of figure 9 are re-presented on figure 20 for comparison. Also given are an *ad hoc* series of results obtained in a mixture of paraffin oil

and turpentine having a viscosity 14·8 times greater than turpentine alone. These latter results follow the theoretical curve remarkably closely. The others appear to asymptote to a time somewhat shorter than that theoretically predicted for complete evolution and phase reversal. In figure 21 the apparent experimental asymptotes (solid lines on figure 9) are compared with the theoretical time for complete evolution of inviscid oscillation as a function of forcing amplitude α. The theoretical curve lies close to an inverse $\frac{2}{3}$ power dependence upon α, and the experimental values are parallel to this but displaced by a factor of about 1·2.

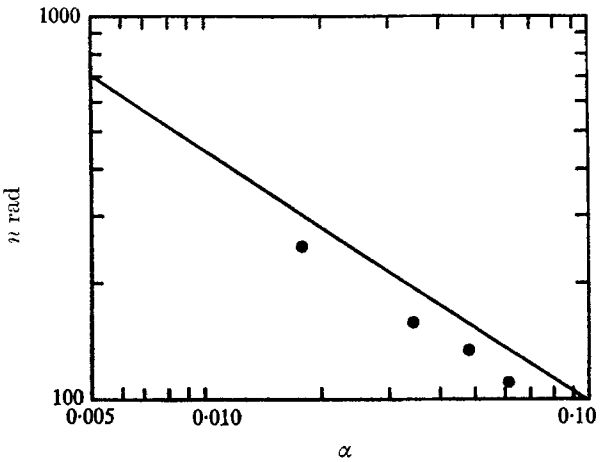

FIGURE 21. Evolution cycle time, $R \to \infty$, compared with experimental asymptote for collapse, as indicated by solid lines in figure 9.

3.1.4.2. *Discussion of the analysis.* The analysis had the heuristic purpose of identifying the non-linear processes controlling the evolution of a *strong* resonant oscillation, and to this end it is a reasonable prolegomenon to immensely more complicated formal treatment. The simplifications made are, however, vulnerable to criticism, and it is worthwhile first to comment on them.

The most important simplification is the assumption that the impulsive retrograde azimuthal motion alone causes the phase shift of the resonant oscillation relative to the existing disturbance. It was pointed out earlier, and the experimental data in tables 3, 4 and figures 14, 15 confirm, that the rate of change of phase is too rapid to be accounted for by linear viscous modification to the resonance geometry, though this modification would bring about a similar but much slower phase shift in the initial stages of evolution. The assumption therefore seems tenable. The difficulty arises, however, in supposing that, whatever the spatial non-uniformities in the azimuthal convection (and table 3 shows that these are considerable), the oscillation field remains linearly associated with the net rate of convection. Much more experimental work is needed to establish the strength of the association. It can only be noted now that the number of container revolutions theoretically predicted to occur for a given phase change (listed in the last column, table 3) lies between the extremes observed, and the excellent agreement between theory and experiment in the number of container

revolutions to peak amplitude (figures 18 and 19) *indirectly* suggests that the oscillation field *effectively* changes its phase at the predicted 'mean' rate.

The second simplification is the use of the 'steady' field description to calculate the net energy of the oscillation field and the torque created on the top plane. When the oscillation becomes larger than $O(\alpha)$ the simplification would result mainly in an error in numerical factors and not in the form of (3.15) and (3.16) so long as the linear field description continued to apply. Before the oscillation becomes large, the presence of forced and initial modes of comparable magnitude and orthogonal in phase cause the phase of the net oscillation measured at a point to vary from the assumed $\psi = 0$ attitude. These are the main cause of the initial phase fluctuation seen in figure 14.

Note that in the absence of viscosity the dimensionless time for evolution must be independent of the representative velocity scale chosen, since Ω is then the only time scale. Thus, an error in velocity scale would be undetectable from measurement of the time to peak amplitude, and would show as a linear factor on the amplitude and Reynolds number scales in solution graphs such as figures 18 to 20. This means that inaccuracies in the numeric factors in (3.15) and (3.16) merely shift the curves without appreciably changing their form. Hence, the inadequate agreement between theory and observation in respect of the dependence of oscillation amplitude upon forcing amplitude α (see figure 16) cannot be resolved, and points to a shortcoming of the analysis.

The third simplification is the adoption of the Stokes solution to give the wall boundary-layer dissipation; this could result in a small error in the third numerical factor in (3.15) and (3.16). In addition, there might also appear a factor containing the Reynolds number to a negative power greater than $-\frac{1}{2}$, owing to the presence of 'inner' wall layers and internal shears. It is unlikely that these latter factors would materially affect, over the range of interest, the character of the dependence of the solution upon Reynolds number, which is generally in good agreement with experiment.

3.1.4.3. *Resonant collapse.* The analysis could not be expected to model the oscillation far beyond the amplitude peak not only due to the influence of 'spin up' viscous modes emerging in time $O(R^{\frac{1}{2}})$ but because a decrease in amplitude implies the transfer of momentum from the oscillation to the mean motion, a process during which the irreversibilities in the oscillation due to viscous dissipation and distortion would inevitably become apparent as the amplitude diminished. In the experimental observations, the amplitude fell below the peak before collapse (see figure 14) but did not approach zero, though the phase followed the theoretical evolutionary cycle. Neither did the collapse immediately follow the attainment of peak amplitude.

One further experimental observation is worth mentioning. For column heights reduced slightly below the inviscid resonant height, collapse was found to occur slightly more *rapidly* than for the inviscid resonance height and peak amplitudes were greater (see e.g. figure 12), the latter being apparently because the free oscillation then has a frequency closer to the net rotation frequency, causing a slower net movement of the oscillation relative to the top. Under this condition, the net phase ψ relative to the top might never

become appreciably greater than $\frac{1}{2}\pi$, and the situation would in principle tend to *stabilize* the oscillation at some finite value (increases in amplitude causing prograde net phase shift, decreases giving retrograde shift from some small positive $\cos\psi$ position). So it is not defensible to propose that collapse is associated solely with the decay of the amplitude to some 'critical' level, or with the particular value of phase of the oscillation relative to the container. As the phase also defines the rate of energy transfer from the oscillation back into the mean motion (at least so long as the oscillation resembles the inviscid form), the likelihood of there being a 'critical' energy transfer rate must also be disregarded.

The only feature of the theoretical solution, compatible both with the phase measurements and the last-mentioned observations, is that collapse may be associated with a phase maximum, a lull or reversal in the mean *net* direction. Where such a lull does not occur, for sufficiently low Reynolds number, the azimuthal convection rate stabilizes finally at some low level in accordance with the observations of § 3.1.3 without resonant collapse. On the basis of the present experiments there is no other identifiable property of the flow field with which the phenomenon of resonant collapse can be associated so consistently, but it is noted that the role of azimuthal convection has not been investigated. The presence of non-uniformities implies 'latitudes' of prograde and retrograde convection when the net convection is small. However, these non-uniformities evidently do not bear simple relationships to the inviscid oscillation field, and the question of how or whether these might bring about destabilization is not tackled. Indeed it is possible that the correspondence between the times for theoretical evolution and experimental collapse is purely coincidental, but it is, nevertheless, germane to make the comparison.

Maintenance of the oscillation after collapse must be brought about at further expense to the angular momentum of the fluid cylinder, this in turn being sustained by 'spin up' for the container walls. Unless a continuous balance can be held between the regeneration and dissipation, the collapse process will repeat itself indefinitely, since for sufficiently great forcing amplitudes a resonant oscillation will be able to energize itself to an extent where it effects the mean rate of rotation in a time shorter than the spin-up time. There is no reason to suppose that the limits on α and Reynolds number for both the initiation and sustenance collapse are the same, but in the present experiments, once the collapse mode appeared, laminar oscillation was never observed to resume.

4. Concluding remarks

The present experiments have found that, at sufficiently high Reynolds numbers, the linear inviscid theory for steady inertial oscillation predicts very accurately the geometrical conditions for resonance of individual modes in a rotating cylinder containing a real viscous fluid, and defines the broad features of the spectrum of oscillation amplitude with column height. The visualizing technique employed was particularly appropriate for the identification of the numerous resonances and for revealing and establishing the direction of discontinuities in

field across characteristic surfaces. However, while the observations confirmed the dependence of discontinuity thickness scale on Reynolds number, they did not support Wood's prediction that imperfect corner reflexion would produce many parallel surfaces undiminished in strength. It seems possible that attenuation or distortion in the locality of reflexion lines has a part to play in the weakening of reflected characteristics.

The effects emerging with resonance of the lower modes of oscillation (such that the amplitude becomes comparable to Ωa) impose a limit on the applicability of the inviscid theory in real situations. A retrograde azimuthal circulation, whose presence is necessary both as a result of the initial generation of the oscillation and for its subsequent sustenance against viscous boundary dissipation, appears, from the evidence of an equation representing the gross balance of energy in the fluid system, to be primarily responsible for the regulation of oscillation amplitude of large amplitude resonances, dominating the more direct viscous effects anticipated by the inclusion of dissipation in the perturbation motion equations. The azimuthal circulation appears to be associated with the phenomenon of 'resonant collapse', in which unsteadiness and disorder abruptly appear on a previously laminar oscillation field. This is evidently not the emergence of shear generated instability and degeneration to turbulence, but is associated with a maximum in the phase of the oscillation relative to the forcing disturbance.

More rigorous analysis is needed in support of the present approximate energy equation, but it is suggested by this and the experiments performed that, at least in situations where the excitation of inertial oscillations is direct (i.e. by rigid boundary distortion), as occurs e.g. in the nutation of liquid filled gyroscopes and projectiles, a truly steady state of inertial oscillation cannot be realized, if the Reynolds number is greater than a critical value.

The author thanks Dr W. W. Wood and Dr P. G. Baines for introducing him to the subject, and for their many valuable comments in the course of the work. He also thanks Mr W. K. Melville, who collaborated in the first successful visualization of the characteristic surfaces. The work was performed at the Aeronautical Research Laboratories, Melbourne; the author acknowledges this institution's permission to publish.

REFERENCES

ALDRIDGE, K. D. & TOOMRE, A. 1969 *J. Fluid Mech.* **37**, 307–323.

BAINES, P. G. 1966 *Aust. Dept. of Supply, A.R.L. Aero Note* 263.

BAINES, P. G. 1967 *J. Fluid Mech.* **30**, 533–546.

BJERKNES, V., BJERKNES, J., SOLBERG, H. & BERGERON, T. 1933 *Physikalisch Hydrodynamik*, pp. 465–471. Berlin: Springer.

BRETHERTON, F. P., CARRIER, G. F. & LONGUET-HIGGINS, M. S. 1966 *J. Fluid Mech.* **26**, 393–410.

BUSSE, F. H. 1968 *J. Fluid Mech.* **33**, 739–751.

FULTZ, D. 1959 *J. Meteor.* **16**, 199–208.

GOLDSMITH, H. L. & MASON, S. G. 1962 *J. Fluid Mech.* **12**, 88–96.

GREENSPAN, H. P. 1964 *J. Fluid Mech.* **20**, 673–696.

GREENSPAN, H. P. 1968 *The Theory of Rotating Fluids*. Cambridge University Press.

JOHNSON, L. E. 1967 *Proc. I.U.T.A.M. Symposium on Rotating Fluid Systems, La Jolla, Calif., April* 1966, pp. 85–106.

KARPOV, B. G. 1965 *Ballistic Research Labs. (Maryland, U.S.), Report* BRL R 1302.

KELVIN, LORD 1880 *Phil Mag.* **10**, 155–168.

MALKUS, W. V. R. 1968, *Science*, **160**, 259–264.

MCEWAN, A. D. 1968 *Aust. Dept. of Supply, ARL Report. Aero.* 134.

OSER, H. 1958 *Z. Angew. Math. Mech.* **38**, 386–392.

STEWARTSON, K. 1959 *J. Fluid Mech.* **9**, 577–592.

WOOD, W. W. 1965 *J. Fluid Mech.* **22**, 337–346.

WOOD, W. W. 1966 *Proc. Roy. Soc. Lond.* A **298**, 181–212.

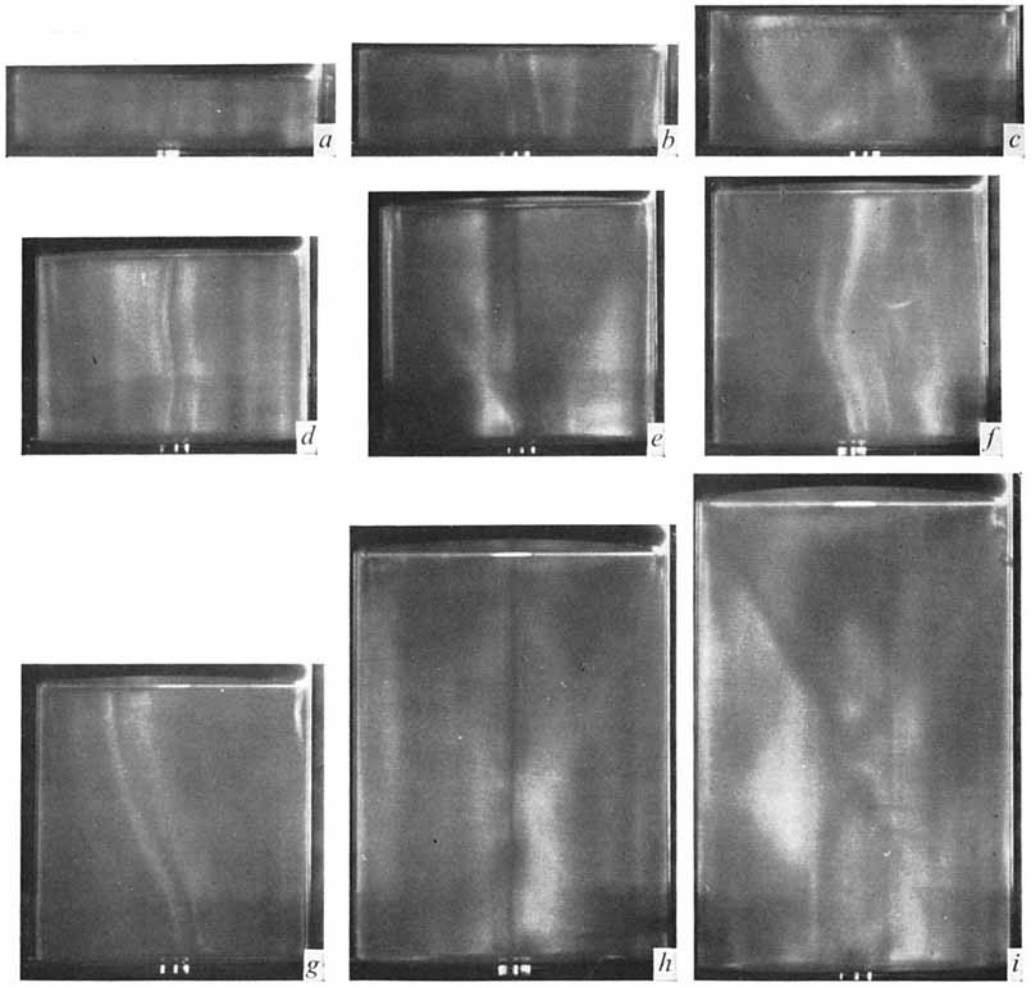

FIGURE 2. Secondary flow patterns as a function of cylinder geometry. $\sigma = \Omega$. Disturbance amplitude $\alpha = 0{\cdot}0344$; $\phi = 0$ at left; rotation = 23·2 rad/sec, anticlockwise from above; illumination from right.

(*a*)	$l/a = 0{\cdot}451$	$\tau = 10$ sec	$\lambda_4 m_1$ resonance
(*b*)	0·613	10	$\lambda_3 m_1$ resonance
(*c*)	0·866	15	$B/T = 1/2$
(*d*)	1·366	20	$\lambda_4 m_3$ resonance
(*e*)	1·732	23	$B/T = 1/1$
(*f*)	1·855	6	$\lambda_3 m_3 + \lambda_2 m_2$ resonance
(*g*)	1·993	2	$\lambda_1 m_1$ resonance
(*h*)	2·61	27	No resonance
(*i*)	2·99	21	No resonance
(*j*)	3·08	23	$\lambda_3 m_5$ resonance
(*k*)	3·46	τ not recorded	$B/T = 2/1$
(*l*)	4·00	4	$\lambda_1 m_2$ resonance
(*m*)	4·46	40	No resonance
(*n*)	4·58	9	$\lambda_4 m_{10}$ resonance
(*o*)	5·20	37	$B/T = 3/1$

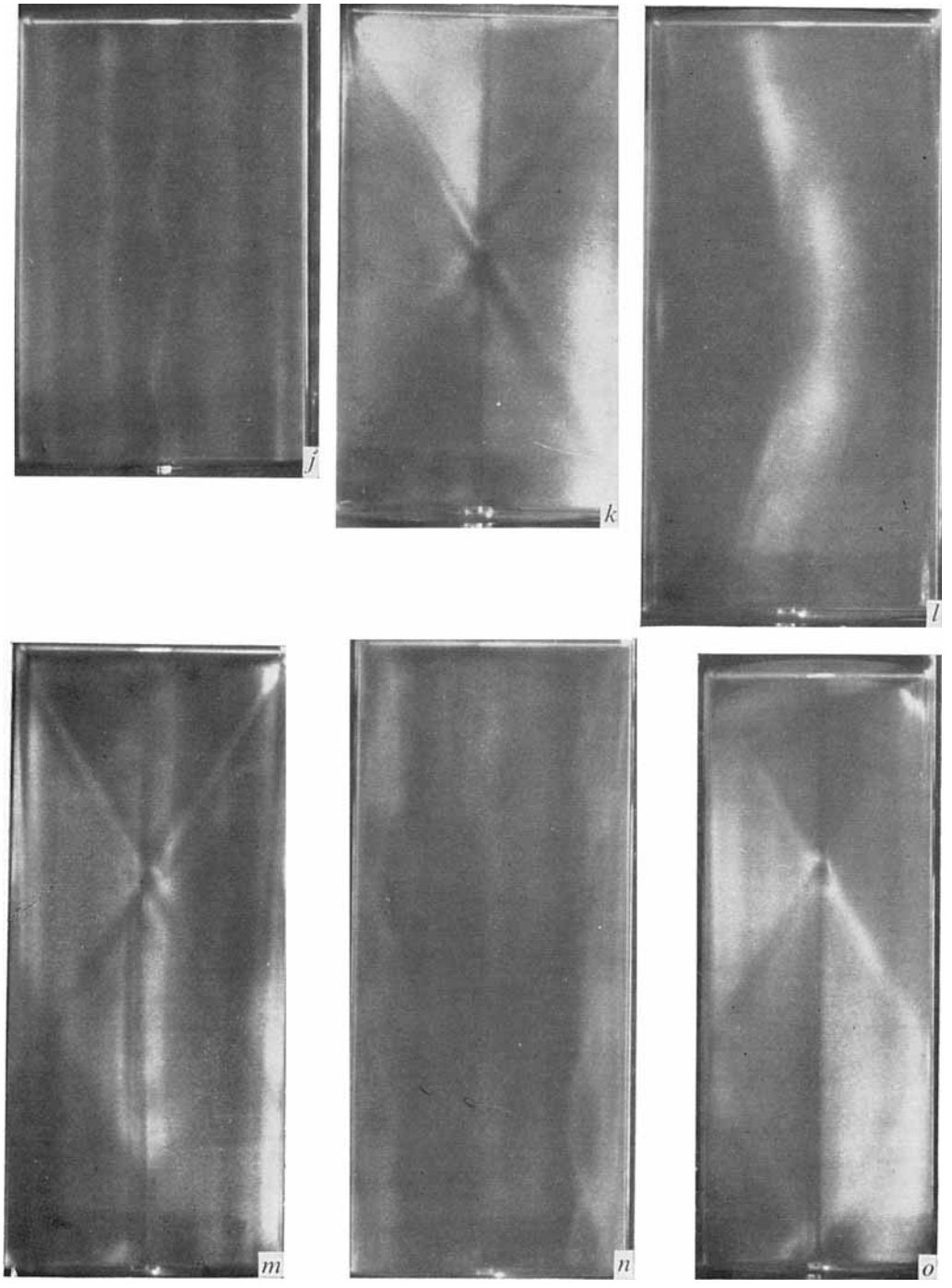

FIGURE 2(*j*)–(*o*). For legend see plate 1.

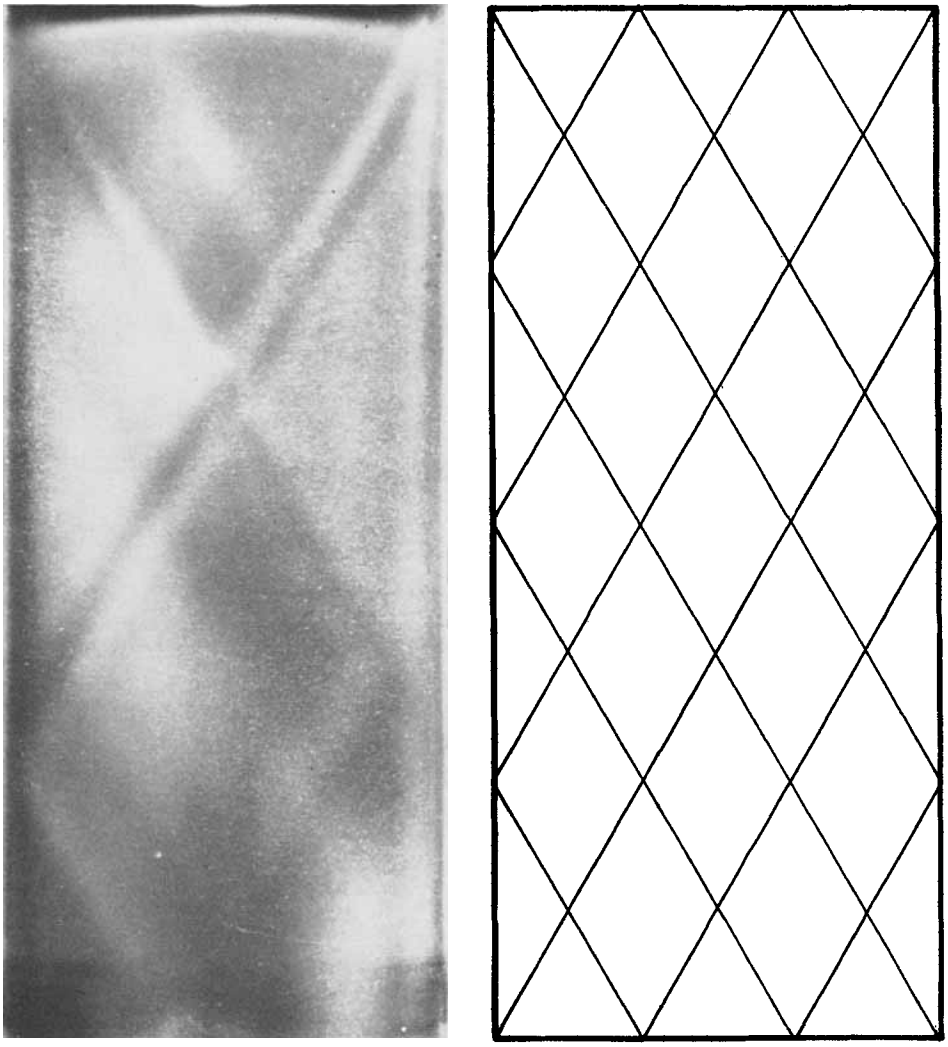

FIGURE 3. Characteristic patterns for $l = (8\sqrt{3}/3)\,a$. Theoretical array of velocity discontinuities compared with experiment.

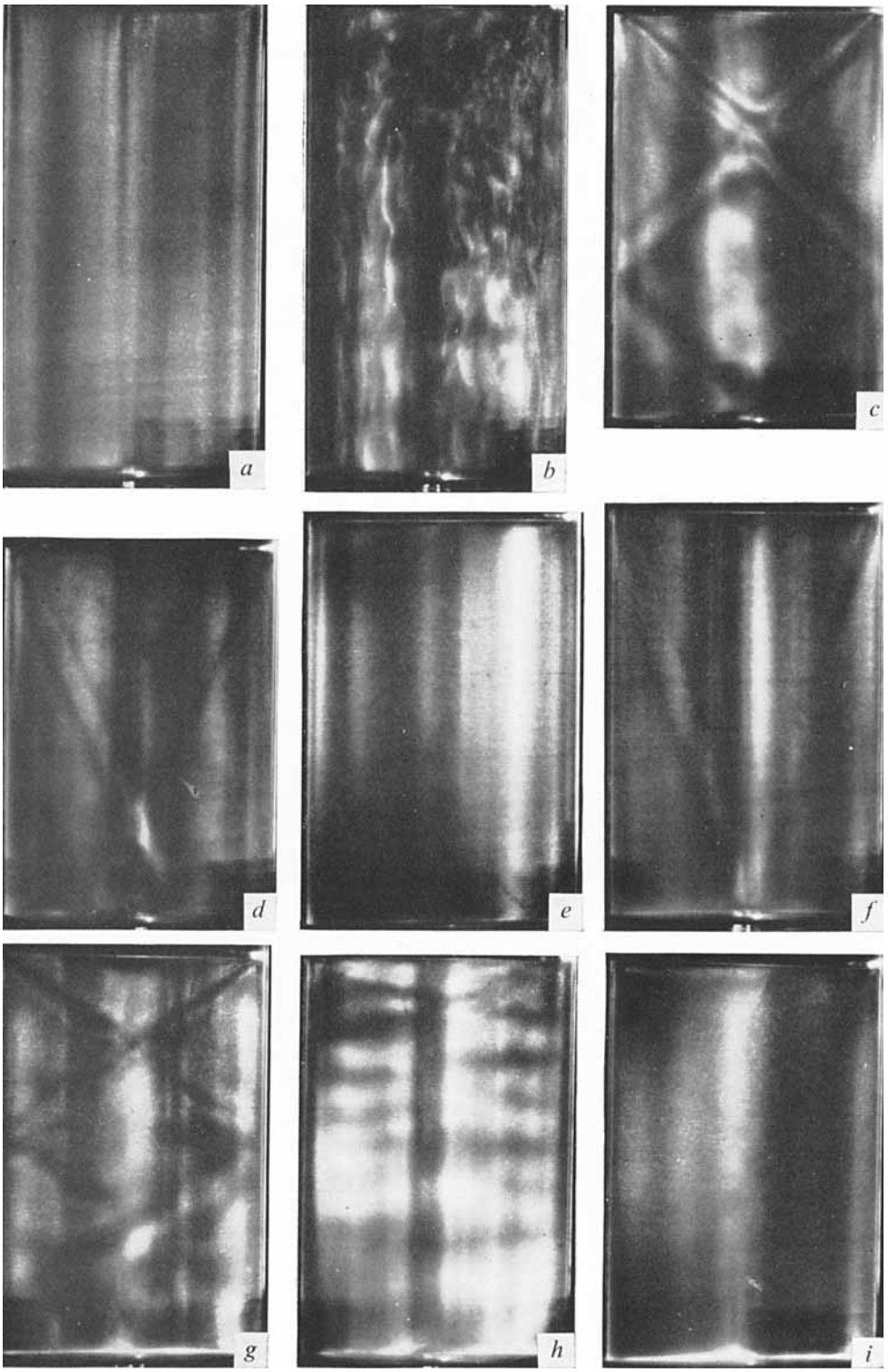

FIGURE 5. For legend see facing page.

FIGURE 5. Characteristic patterns for $-2 < \sigma/\Omega < 2$. Disturbance amplitude $\alpha = 0{\cdot}034$. Illumination from right. Rotation A.C.W. from above.

(*a*)	$\sigma/2\Omega = 1{\cdot}072$	$\Omega = 22{\cdot}4$ rad/sec
(*b*)	$0{\cdot}978$	$22{\cdot}6$
(*c*)	$0{\cdot}700$	$22{\cdot}6$
(*d*)	$0{\cdot}414$	$22{\cdot}6$
(*e*)	$0{\cdot}0092$	$22{\cdot}7$
(*f*)	$-0{\cdot}296$	$23{\cdot}0$
(*g*)	$-0{\cdot}828$	$13{\cdot}7$
(*h*)	$-0{\cdot}928$	$23{\cdot}1$
(*i*)	$-1{\cdot}031$	$13{\cdot}7$

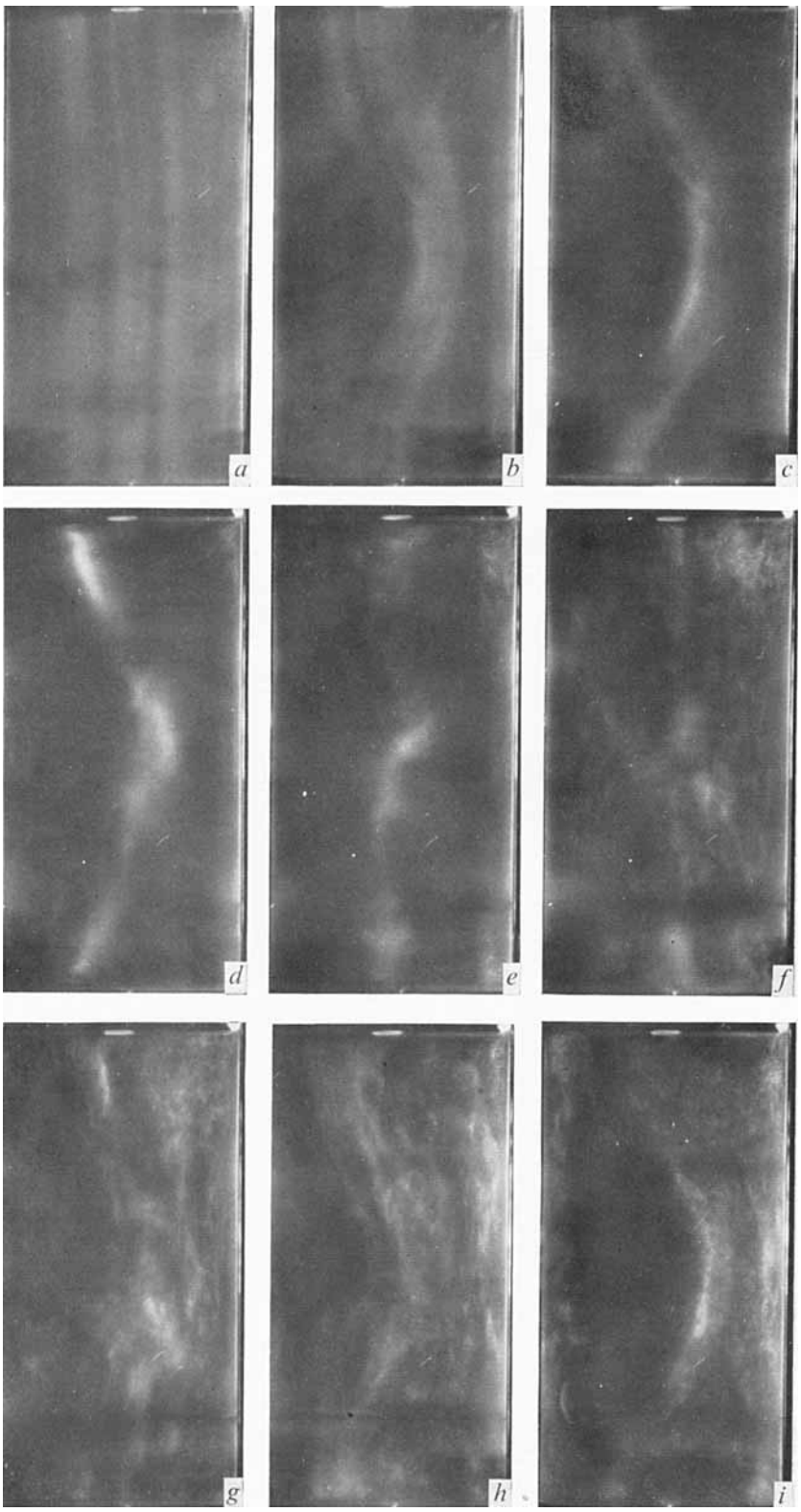

FIGURE 7. For legend see facing page.

FIGURE 7. Stages of resonant collapse, $\lambda_1 m_2$ mode.
$\alpha = 0{\cdot}063$, $R = 4{\cdot}8 \times 10^4$.

(*a*) 0 rev of container
(*b*) 4·4
(*c*) 8·3
(*d*) 12·6
(*e*) 16·7
(*f*) 20·3 rev of container
(*g*) 24·6
(*h*) 29·0
(*i*) 32·6

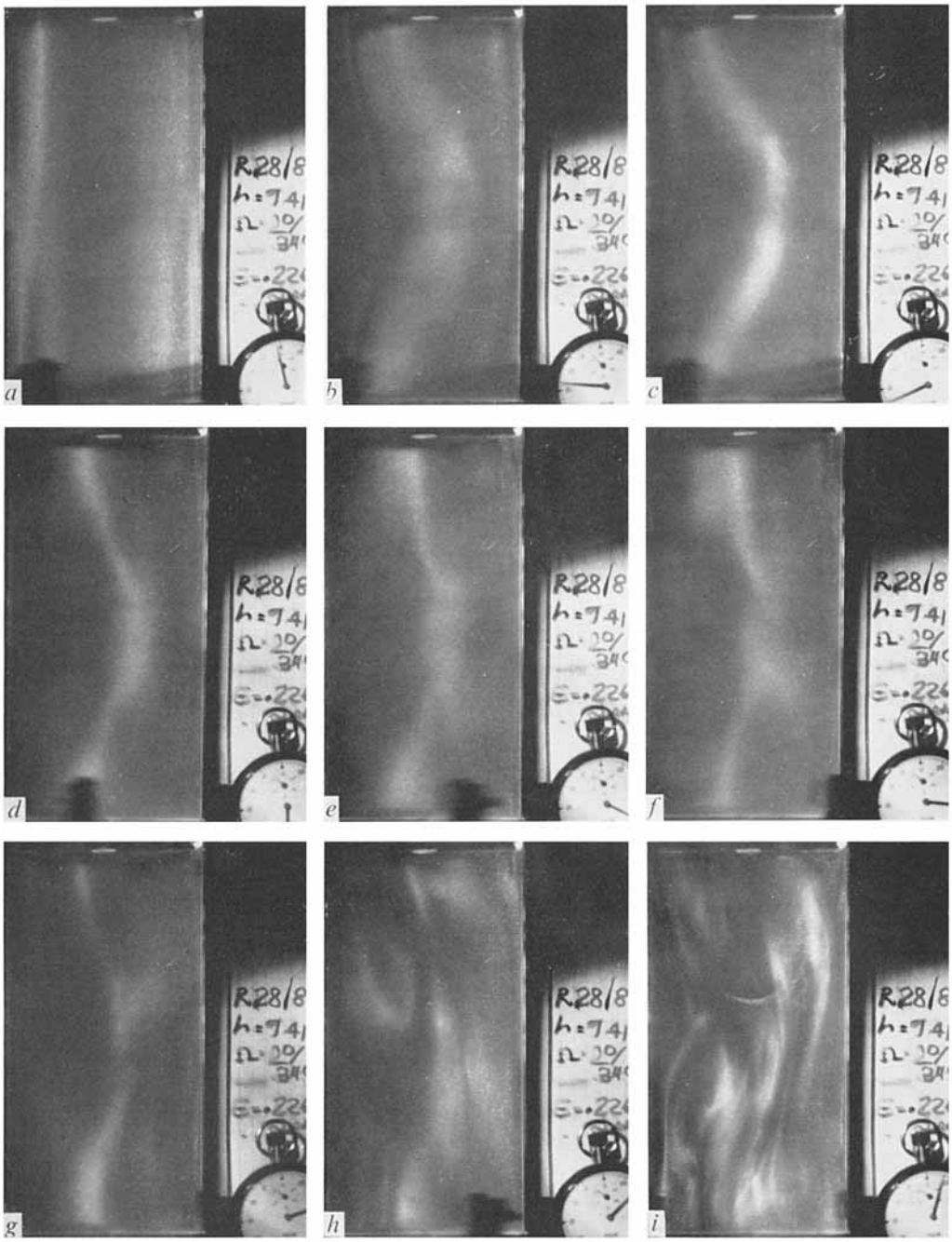

FIGURE 8. Stages of resonant collapse $\lambda_1 m_2$ mode.
$\alpha = 0{\cdot}063$, $R = 7{\cdot}8 \times 10^3$.

(*a*) 0·59 rev of container
(*b*) 7·9
(*c*) 10·9
(*d*) 17·3
(*e*) 22·8
(*f*) 25·1 rev of container
(*g*) 27·4
(*h*) 30·1
(*i*) 33·2